Eksploatacja i Niezawodnosc - Maintenance and Reliability

Volume 29 (2027), Issue 2

https://ein.org.pl

The Polish Maintenance Society

Operation of integrated electronic security systems in a distorted railway electromagnetic environment – selected security aspects

Kamil Białek[1], Patryk Wetoszka[1], Jacek Paś[2], Adam Rosiński[3,*]

[1] Signalling and Telecommunications Laboratory, Railway Research Institute, Poland
[2] Faculty of Electronic, Military University of Technology, Poland
[3] Department of Air Transport Engineering and Teleinformatics, Faculty of Transport, Warsaw University of Technology, Poland
* Corresponding Author: adam.rosinski@pw.edu.pl

Received: 24 May 2026
Revised: 8 July 2026
Accepted: 30 August 2026
Online: 14 September 2026

Abstract

This research paper reviews issues associated with identifying the impact of electromagnetic interference (EI) sources within an environment where integrated electronic security systems (IESS) are operated. IESS are operated under diverse environmental conditions. They are exposed to internal and external EIs both natural and artificial. The authors conducted experiments within a natural environment. They enabled identifying these interference sources. The outcome of field environmental tests, followed by the modelling of an IESS reliability and operation process was a conclusion that there are methods to minimise encountered EIs. The application of technical solutions within internal IESS structures increases the probability of a system remaining in a state of full fitness. The considerations in this article allowed to develop a method to assess the impacts of EIs on IESS. This method can be successfully employed to examine the operation process in other electronic systems and devices.

Keywords: *operation process, integrated electronic security systems, electromagnetic environment, interference, operation process model*

Article citation:
Białek K, Wetoszka P, Paś J, Rosiński A, Operation of integrated electronic security systems in a distorted railway electromagnetic environment – selected security aspects, Eksploatacja i Niezawodnosc – Maintenance and Reliability 2027: 29(2) http://doi.org/10.17531/ein/235818

Highlights

- Identification of electromagnetic interference sources.
- Electromagnetic interference process.
- Models of electromagnetic interference impacts on integrated electronic security systems.
- Determination of safety indicators for the operation of electronic security systems.
- Minimisation of electromagnetic interference impact.

1. Introduction

Integrated electronic security systems (IESS) involve the application of comprehensive technical solutions that utilise available protection subsystems within their internal functional structure [1,2]. These subsystems, employed as a whole to ensure an appropriate security level include, among others, Access Control Systems (ACS), Closed-Circuit Television (CCTV), Intrusion Detection Systems (IDS), Audio Warning Systems (AWS) and one of the main subsystems, namely, the Fire Alarm System (FAS) [3–5]. All of the aforementioned subsystems are properly organised and technically coupled into a single structure that is centrally managed as a unified whole. An IESS can be monitored – managed at the installation site of specific security subsystems (e.g., in a protected building or remotely, with the use of independent transmission lines connected with an Alarm Receiving Centre (ACR). In most cases, local monitoring, management, as well as servicing and repairs within a specific time associated with all security subsystems is implemented in the case of building (facilities, vast areas) that are classified as the so-called State Critical Infrastructure (SCI) [6,7]. This requires a pre-defined failure response time associated with a given subsystem. Other IESSs offer the possibility of remote monitoring via ACR, i.e., arrival and implementation of, e.g., service activities, within a specific, pre-set time period. The main task of IESSs organised in such a manner is ensuring improved functional efficiency of all subsystems. This includes, e.g., reduced time required for external and internal actions, i.e., response to threats of fire, intrusion, burglary, assault, etc., as well as obtaining full control over the security of a building, facility or vast area, usually from a single operator station equipped in systems visualising unwanted events [3,8,9]. Such mutual technical arrangement of all security subsystems leads to an increased protection (safety) level and optimises operational processes associated with, e.g., monitoring, management, logistics, recovery and servicing, as well as power supply. All IESSs operate and fulfil their operational duties within a given, favourable or unfavourable, natural environment, that includes all changes of weather conditions, such as temperature, atmospheric pressure, humidity, precipitation, snowfall, as well as fog, rime or air pollution. These are classified as external environmental impacts, and have to be considered by an IESS designer as part of a specific operational process. However, there are also frequent impacts (environmental changes) that are not taken into account in a given operational process [10–12]. It is a generally understood electromagnetic phenomenon that coexists within a specific area, protected buildings or over a vast space accommodating, e.g., operated technical installations of ICT and communication systems, radar stations, LV, MV and HV contact and traction lines, as well as railway traffic control systems in the case of railway areas [8,13–15]. All these technical systems must coexist within such an environment and correctly operate even in cases of exceeded permissible electromagnetic field parameter levels specified in particular regulations, provisions or technical standards, i.e., electric (E) and magnetic (H) field strengths [16–19]. Coexistence of various technical systems within a specific, protected natural environment is known as overall electromagnetic compatibility [20–22]. The concepts of internal and external compatibility have to also be distinguished and taken into account for different technical systems operated in a building or over a vast area. Such systems consume either very low supply current, in the order of μA, mA (these include sensors, modules, detection circuits and lines, etc., IESSs) or very high supply current in the order of kA in the case of industrial power lines or rolling stock supply traction lines [23–25]. All employed technical systems, also those responsible for security, should function correctly in a given, distorted natural electromagnetic environment [26–31]. Earth's electromagnetic environment is distorted intentionally and purposefully, by using, e.g., TV and radio transmitters, radar stations, and wireless communication and telephony [32–40]. However, the environment is also distorted unintentionally, e.g., as an electric or magnetic field, around supply line cables or railway traction lines that consume very high current. Electromagnetic interference sources can be stationary (e.g., communication system antennas and transmitters) or non-stationary, mobile over a protected area – e.g., railway vehicles – traction units that use the contact line to draw current in the order of hundreds of kA to start and run electric drive motors with a capacity of several – several hundred MW [6,41–43]. Fig. 1, simplified for the sake of clarity, shows a technical IESS embodiment, employed within a railway area and describes the concept of internal and external electromagnetic compatibility.

Employing IESS for protecting buildings and vast areas with other facilities that require ongoing monitoring (Fig. 1) contributes significantly to improving the overall safety level [44–48]. This refers to adverse external and internal impacts – e.g., burglary and intrusion detected by an IDS, while simultaneously confirmed by two systems, namely, CCTV and ACS. In this case, the physical security staff in the facility does not need additional time to recognise a threat and immediately takes action associated with eliminating it [49,50]. Employing IESSs to ensure an appropriate security level is shown in Fig. 2 for various factors impacting a protected facility.

In order to provide an appropriate security level, the facility had been equipped with an IESS covering the following systems: FAS, AWS, IDS, CCTV, ACS [4,51,52]. All employed ESSs are characterised by high resistance to external and internal natural environment interference (change in temperature and humidity, lightning discharge, etc.) and variations in the surrounding electromagnetic environment (EI) arising from radiating natural and artificial sources found on Earth – stationary and non-stationary in the case of railway areas in question. All employed IESSs (FAS, IDS, …, ACS) are tasked with maintaining a preset security level presented in Fig. 2 as an inclined plane. Selecting a proper design, including various ESS organisational and technical solutions and anti-destructive devices contributes to maintaining a pre-set security level, also in the light of adverse EI impact [53–55]. Fig. 2 shows three different cases (a, b and c) of adverse external and internal factors impacting an operated IESS. In the case of a), the existing internal and external interference level causes a violation of the IESS security level.

This was illustrated through a deflection from the inclined plane equilibrium. All employed technical, structural and organisational solutions, including anti-destructive systems and elements, do not lead to an interference level reduced to such required for the correct ESS operation within the protected building [10,56–58].

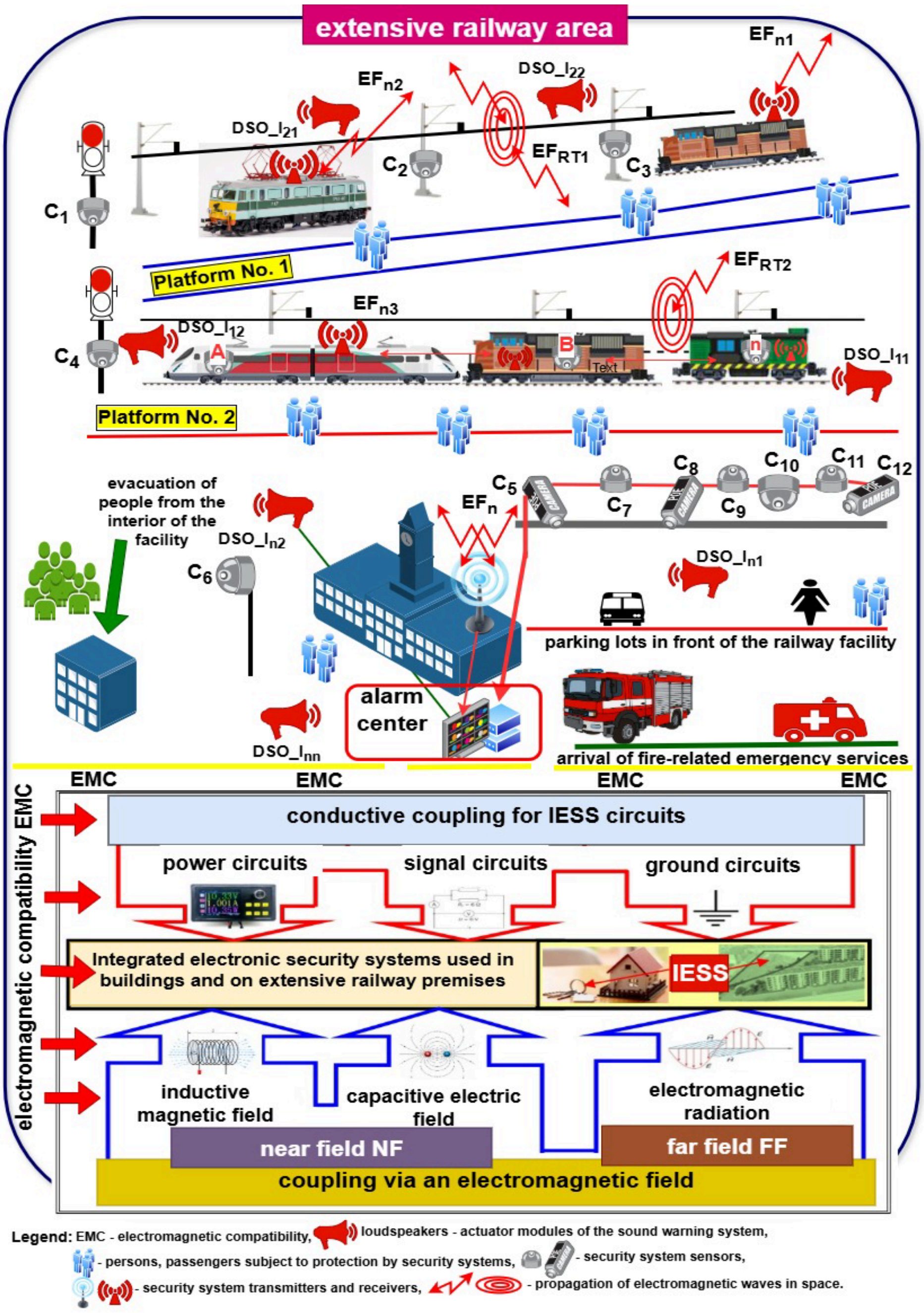

Figure 1. Distorted electromagnetic environment over a vast railway area, where: EF_{n1}, EF_{n2}, EF_{n3}, EFn4, EF_n – electromagnetic field generated by security system transmitters, EFRT1, EFRT2 – unintentional electromagnetic field generated by electric railway traction supplying rail vehicles, C_1, C_2, C_3,…,C_{12} – CCTV cameras, DSO_I_{11}, DSO_I_{12}, DSO_I_{21}, DSO_I_{22}, DSO_I_{n1}, DSO_I_{nn} – Audio Warning System loudspeakers, IESS – Integrated Electronic Security Systems, EMC – electromagnetic compatibility, NF – near field, FF – far field, person No. 1, No. 2.

In the case of Fig. 2 b) and c), the impacting interference does not result in a security level change. If appropriate technical and organisational solutions are employed (such as in Fig. 2b), an IESS is able to automatically recover to a security level status. This means the absence of adverse external and internal, natural or artificial, intentional and unintentional, and finally stationary or non-stationary interference (sources) [59–61]. An assumed IESS security level is impacted not only by unintentional external and internal interference but also unfitness cases encountered in individual security systems [7,62,63,64]. Such unfitness cases may be the reason behind a security level change, i.e., lead to an undesirable variation in the inclined plane equilibrium, without the possibility of spontaneous equilibrium recovery – Fig. 2c). A recovery is then feasible after implementing a recovery process by a service team located within the protected facility. In addition to previewing the impact of electromagnetic interference on IESS operation process, the research paper also contains a critical review of source literature in this field [65,66,67]. A significant section of the paper covers a study of electromagnetic interference (EI) over an entire frequency range, conducted at an experimental range and on actual communication routes [68,69]. An analysis of received results enabled reliability and operation process modelling and determining the coefficients of EI impact on the operation process. The last chapter focuses on a computer simulation and contains conclusions related to the operation process of selected IESSs. Therein, the authors also determined the impact of EI on the operation process of selected IESSs for developed security system models [70–72].

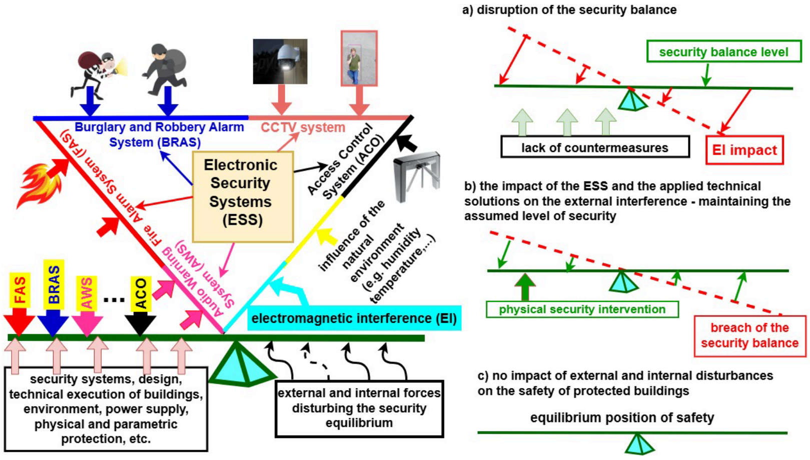

Figure 2. Impact of adverse external and internal interference on IESSs operated within a protected facility; change in impact factors directly associated with employed ESSs – e.g., burglary, fire, smoke, breached observation zone, etc. This also includes a change in natural environment parameters and the impacting electromagnetic field over the entire frequency range.

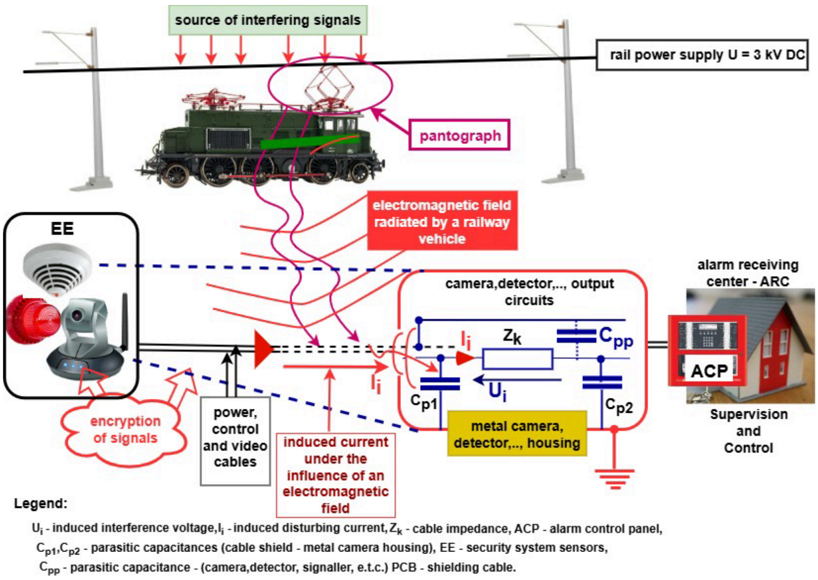

Figure 3. Model showing the impact of unintentional, non-stationary electromagnetic interference on ESS components caused by locomotives on a railway track.

The article discusses studies on the impact of electromagnetic interference generated over a vast area on electronic security systems (ESS). Further research and papers will separately address studies related to unintentional generation of electromagnetic interference associated with locomotives and electric track vehicles. Fig. 3 illustrates a model demonstrating the impact of such interference on ESS components. The sources of very high-power electromagnetic interference are the electric motors of locomotives. Upon starting, vehicles consume large volumes of current from the contact line, which then flows through the pantograph supplying the motors. In such a case, a traction unit is the source of non-stationary, unintentional, radiated electromagnetic interference. Due to the current flowing in the circuit, the railway contact line, pantograph and locomotive motor, as well as its value and variability over a rather short period of time, the impact of such interference on ESS component should be considered individually. It is an interference range most usually propagating in the form of an electromagnetic wave above 30 MHz – so-called *radiated* – Fig. 3. Parasitic capacitances C_{p1},C_{p2},C_{pp}, cable or earthing impedance Z_k and mutual inductance of e.g., cables and connections should be considered for this frequency range. Fig. 3 is a simplified illustration of the impact electromagnetic interference has on ESS components near a railway track. As part of further studies, the authors plan to present the results of researching the impact of unintentional, non-stationary interference sources on ESS, i.e., of locomotives drawing different currents from a 3 kV DC contact line, moving at different speeds and with enabled/disabled on-board receivers processing supply voltages.

2. Source literature review

The complex operation process of IESSs operated in protected facilities requires taking a rather broad aspect of their utilisation within the surrounding reality into account [4,32,73]. Simultaneously, this is the impact of an adverse environment:

- natural with fluctuating temperatures, pressure or humidity, but also forced [13,46,74].
- changes in the surrounding electromagnetic environment unintended by the users of means of railway transport [3,70,74].

Globally available source literature contains a rather thorough description of such phenomena as a temperature, pressure or humidity change in the light of their impact on the operation process and the use of electronic elements, devices, modules or systems operated in everyday human life within the surrounding environment [75–77]. The aforementioned technical objects should be resistant, durable and not susceptible to significant changes in natural environmental parameters, particularly in the case of means of land, sea or air transport. Electronic modules and devices often contain embedded local elements (systems) that stabilise the impact of, e.g., a temperature change on a working point in amplifiers, integrated circuits, etc. [62,78,79] In operated electronic systems, their individual modules, the components of such technical objects, are also equipped with devices to protect against the impact of, e.g., temperature on the operating parameters of equipment used. Technical solutions can also be found within IESSs [6,46,80,81]. There is not global solution to this issue, e.g., in alarm control panels (ACP) that are devices determining the development of an alarm signal [13,82,83].

Power supply is also an exceptionally important problem associated with the IESS operation process. It is most often fed from the public industrial power grid [6,45,84,85]. Power supply reliability over a pre-set operating time, when IESS are operating and implementing operational tasks is yet another crucial issue. Power lines experience supply voltage dips, decays, harmonics, and fluctuations, as well as radioelectronic interference concurrent with a utility signal [8,46,69,86,87]. The aforementioned issue is prevented in most cases by applying advanced microprocessor power supplies located inside an ACP with extensive stabilisers and filters with pre-set attenuation bands [7,57,78,88]. Battery banks with a capacity determined based on the energy balance are the most common auxiliary power supply devices for IESSs [9,43,65,88,89].

Moreover, the reliability of IESSs intended for protecting facilities is an additional operational concern. The well-known principle of redundancy is employed to improve the functional reliability of individual IESS components already at the engineering stage, without knowing the purpose and objective of specific modules – Fig. 2 [45,61,69,90,91]. Technical solutions employed in individual ESSs should not experience a so-called critical failure, which determines the 'service life' of an entire security system intended to protect a facility. More and more modern ESS solutions offer an embedded fail-safe principle. This particularly applies to FASs. It also involves 100% duplication of detection lines and circuits (with hooked-up sensors) in IESS structures, which are crucial in the aspect of facility protection [15,52,59]. However, the available source literature lacks the determination of the impact of conducted and radiated electromagnetic interference on the operation process, in particular on the operation process reliability of these IESSs over a given time [59,72,76,92].

The phenomenon of so-called false alarms is a particular operational issue in the case of IESSs. This issue is particularly important in relation to FAS, but not only those systems [4,34,52,70]. Generating a false alarm signal by an FAS often leads to the arrival of the State Fire Service (SFS), the Police and other law enforcement services [14,58,71]. It is also associated with announcing an alarm and evacuation by an AWS. A review of source literature led to a conclusion that there are local solutions to this issue (already in detectors, detection loops – namely, the application of, e.g., multidetectors or coincidence alarming) but also in the ACUs, through the application of the alarm signal confirmation principle [80,93,94]. However, there are no papers or studies on the impact of EI on false signal generation, let alone the 'survival' of individual IESS components or the system as an entirety, and the appearance of strong electromagnetic interference, especially within a so-called railway area, where the Earth's natural environment (E-electric field and H-magnetic field) is particularly distorted [3,45,63,66,95].

A comprehensive study of a distorted electromagnetic environment in so-called railway areas is notably hindered due to actual transport route traffic [62,69,96,97]. The source literature contains studies that focus only on individual frequency bands and generated interference [66,98,99]. However, the impact of such interference, particularly on the operation process of electronic systems or IESSs alone, has not been assessed. The authors of the paper conclude that the source literature contains only study results, e.g., interference signal spectra or amplitudes, while stating that is lacks the assessment of the EI on IESS operation process security [14,49,61,80,92].

3. Electromagnetic interference impacting the operation process of integrated electronic security systems – research results

Natural environment and generated electromagnetic interference impacting IESSs were studied for two different cases, i.e.:

- emission tests of radiated interference over a frequency range of 30 MHz – 230 MHz and within a railway area at a distance of 10 m from a traction substation supplying rail vehicles on a railway route,
- emission tests of radiated interference over a frequency range of 9 kHz – 300 MHz within the premises of the Test Track Centre in Żmigród.

Radiated interference emission for a contact line (railway traction) were measured with supply current at two values, namely, I_1 = 500 A and I_2 = 1650 A. The studies were conducted at the premises of the Test Tract Centre in Żmigród as the impact of a railway system – power supply traction on the natural environment and adjacent buildings with operated IESSs. Emissions of radiated interference in the 30 MHz – 230 MHz frequency range for the second supply current value (I_2) were conducted within a railway area, at a distance of 10 m from a traction substation. Measurements were taken pursuant to the methodology set out in standard PN-EN 50121-2 for the housing port, for a frequency band required by standard PN-EN 50121-2 and under the assumption of permissible radiated interference emission values specified in standard PN-EN 50121-2.

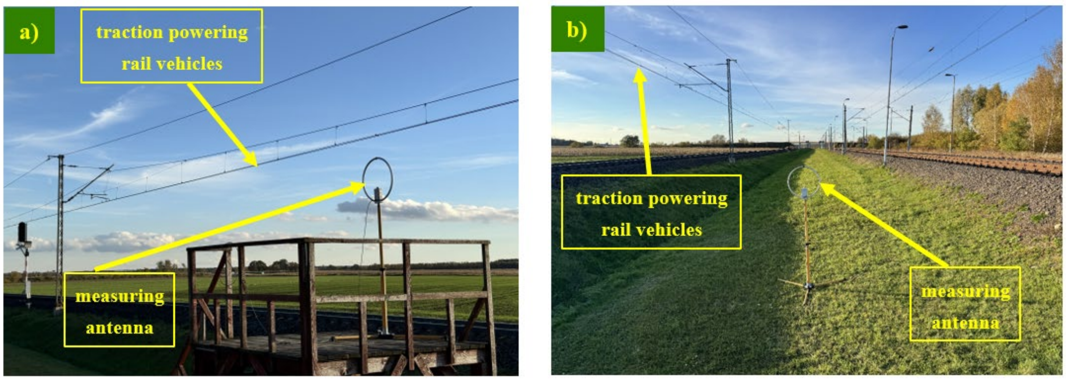

Figure 4. Environment and interference measurement, (a) test bench for measuring radiated interference emissions in the 9 kHz – 30 MHz range, (b) test bench for measuring radiated interference emissions in the (30 – 230) MHz range.

Fig. 4 a), b) shows the arrangement of measuring systems, contact line, railway line and antennas (measuring sensors, interference receivers) related to the measurements for two load cases, namely, I_1 = 500 A and I_2 = 1650 A.

Measurement procedure, antenna polarisations, measurement distance and measuring equipment employed for two power supply (load) cases, I1 = 500 A and I2 = 1650 A, of the railway contact line were described and illustrated in Table 1 to 5, respectively.

Table 1. Contact line frequency bands and operating modes – heating current flow equal to I1 = 500 A.

Frequency range	Contact system operating mode
9 kHz – 150 kHz 150 kHz – 30 MHz	background
9 kHz – 150 kHz 150 kHz – 30 MHz	load – 500 A heating current flow

Table 2. Types, configurations and distances of contact line (catenary) antennas for current flow equal to I1 = 500 A.

Antenna type	Frequency band	Measuring distance from track axis	Antenna suspension height	Antenna orientation/ polarisation
FMZB 1513	9 kHz – 150 kHz	10 m	1.5 m	parallel
FMZB 1513	150 kHz – 30 MHz	10 m	1.5 m	parallel

Table 3. Measuring equipment employed during the tests - heating current flow equal to I1 = 500 A.

Measuring instrument	Model	Manufacturer
Measuring receiver	ESCI3	Rohde & Schwarz
Active loop antenna	FMZB 1513	SCHWARZBECK MESS ELEKTRONIK
Measuring cable	RG58CU/ 11N/11N/ 010000	HUBER SUHNER
Thermohygrobarometer with a display panel	LB-715, LB-755/A	LAB-EL

Table 4. Contact line frequency bands and operating modes – current flow equal to I2 = 1650 A.

Frequency range	Operation mode	Measurement distance	Antenna polarisation
30 MHz – 230 MHz	background load 1650 A	3 m	Vertical (V) Horizontal (H)

Table 5. Measuring equipment employed during the tests – heating current flow equal to I2 = 1650 A.

Measuring instrument	Model	Manufacturer
Measuring receiver	ESCI3	Rohde & Schwarz
Measuring cable 10 m	RG58CU/ 11N/11N/ 010000	HUBER SUHNER
Biconical antenna	VBA 6106A	SCHAFFNER
Log-periodic antenna	VUSLP 9111B	SCHWARZBECK MESS ELEKTRONIK
Thermohygrobarometer with a display panel	LB-715, LB-755/A	LAB-EL

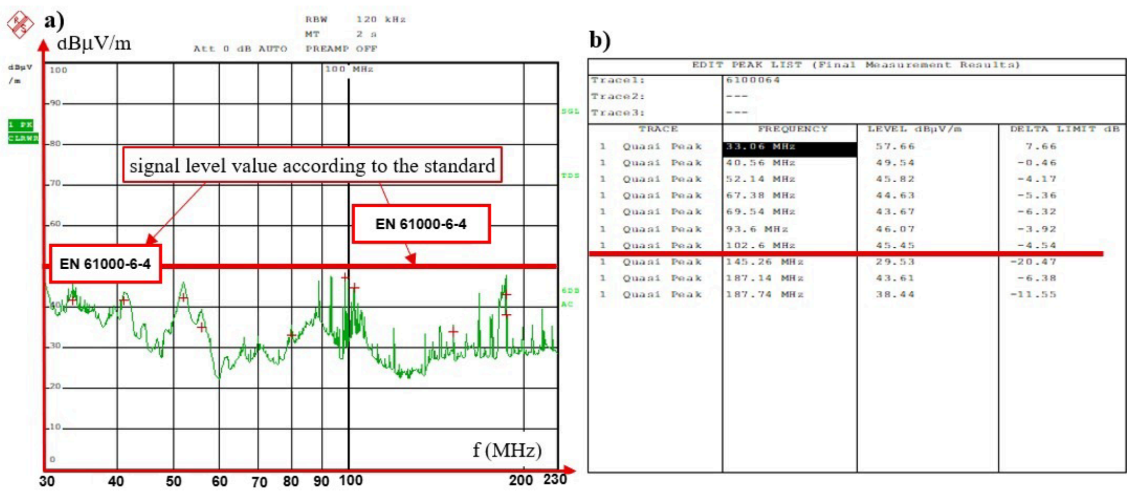

Figure 5. Signal spectra background measurement results without supply current consumption within a given environment, for a frequency range (30 – 230) MHz, V antenna polarisation, (a) signal spectrum, (b) sample interference values for a selected frequency – one measurement case marked for: f = 102.6 MHz, E = 45.45 dBµV/m, delta limit – 4.54 dBµV/m.

Fig. 5 a) and b) show the spectrum of interference signals generated within the environment, so-called electromagnetic field background without active traction power supply, for a current consumption I2 = 1650 A, frequency band (30 – 230) MHz, antenna polarisation V.

Fig. 6 a) shows the signal spectrum background test results without supply current consumption within a given environment, for a frequency band of (30 – 230) MHz, antenna polarisation H, no power supply load from the railway traction side.

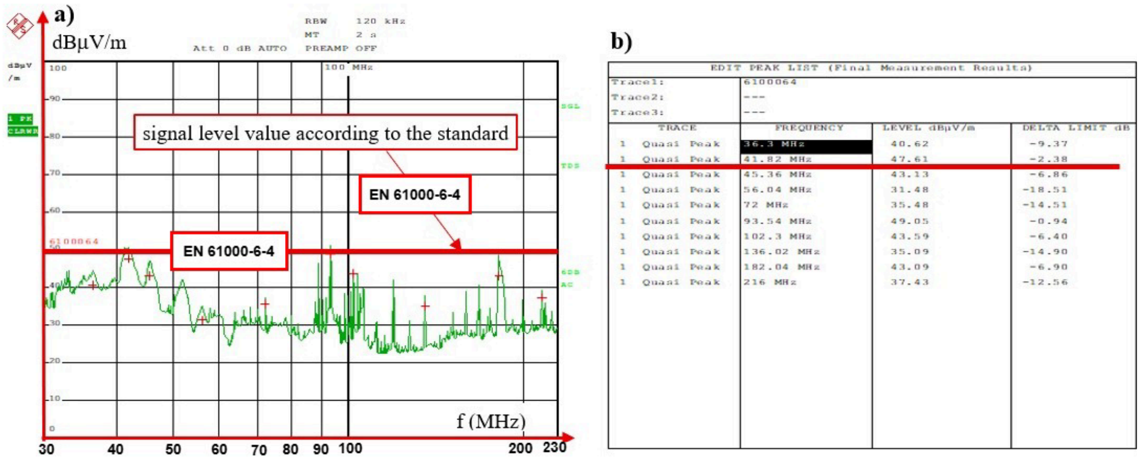

EDIT PEAK LIST (Final Measurement Results)			
Trace1:	6100064		
Trace2:	---		
Trace3:	---		
TRACE	FREQUENCY	LEVEL dBµV/m	DELTA LIMIT dB
1 Quasi Peak	36.3 MHz	40.62	-9.37
1 Quasi Peak	41.82 MHz	47.61	-2.38
1 Quasi Peak	45.36 MHz	43.13	-6.86
1 Quasi Peak	56.04 MHz	31.48	-18.51
1 Quasi Peak	72 MHz	35.48	-14.51
1 Quasi Peak	93.54 MHz	49.05	-0.94
1 Quasi Peak	102.3 MHz	43.59	-6.40
1 Quasi Peak	136.02 MHz	35.09	-14.90
1 Quasi Peak	182.04 MHz	43.09	-6.90
1 Quasi Peak	216 MHz	37.43	-12.56

Figure 6. Signal spectra background measurement results without supply current consumption within a given environment, for a frequency range (30 – 230) MHz, V antenna polarisation, (a) signal spectrum, (b) sample interference values for a selected frequency – one measurement case marked for: f = 41.83 MHz, E = 47.61 dBµV/m, delta limit – 2.38 dBµV/m.

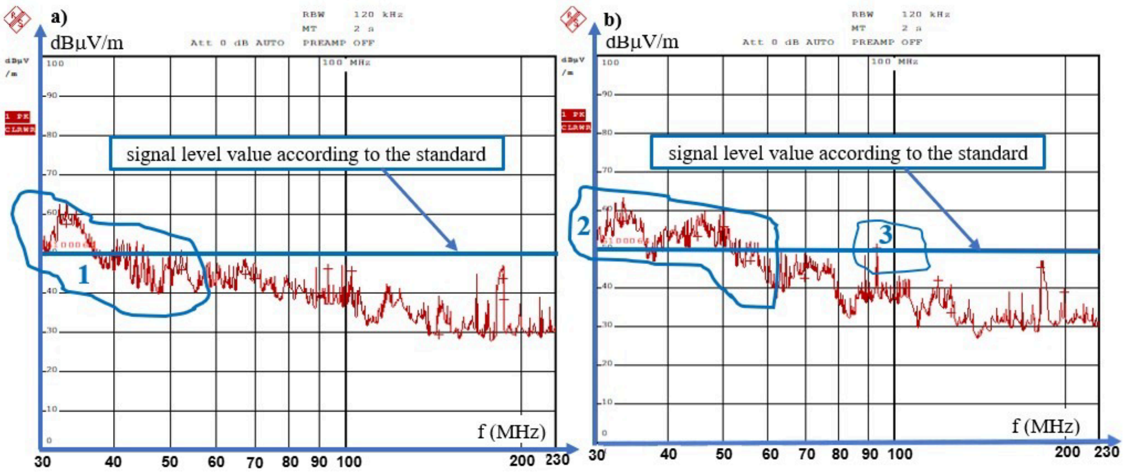

Figure 7. Unintentional electromagnetic field spectrum test results for a frequency range of (30 – 230) MHz, V and H, respectively, antenna polarisation in the cases of contact line power consumption equal to I2 = 1650 A, (a) measurement results for antenna V polarisation, (b) measurement results for antenna H polarisation, measurement for a frequency range of (30 – 230) MHz.

Fig. 5 and 6 do not contain any exceeded values for unintentional interference signals under the applicable EN 6100064 standard, which applies to permissible V and H polarisation limits for electromagnetic environment background surrounding an IESS. Only in the case as in Fig. 5 a) for a frequency f = 94 Mhz, the interference signal value is equal to E = 49.98 dBµV/m. Fig. 7 a), b) shows the electromagnetic field unintentional emissions spectrum test results for the frequency range (30 – 230) MHz, V and H, respectively, antenna polarisation in the cases of contact line power consumption equal to I_2 = 1650 A. As can be noted in Fig. 7, permissible interference levels specified in standards for various frequency ranges have been exceeded both for V and H polarisation, within frequency bands marked in the drawing as 1, 2 and 3. In the case of V polarisation, increased electromagnetic interference values occur in the frequency range from 30 to 52 MHz (area 1) – Fig. a). It is different in the case of the measuring antenna polarisation H vector. In this case, elevated electromagnetic interference values occur for two frequency ranges: from 30 to 57 MHz (area 2), and near f = 93 MHz (area 3). Unintentional radiation standards are particularly exceeded (significant) for the following frequency range: (32 – 38) MHz – Fig. 7a – area 1; (33 – 37) MHz and (45 – 50) MHz – area 2, and 93 MHz – area 3 – Fig. 7b.

Fig. 8 a) and b) show the unintentional electromagnetic field emission spectrum test results for the low frequency range (9 – 150) kHz. Fig. 8 a) shows the electromagnetic field background for this range. In turn, Fig. 8b) shows an electromagnetic field spectrum in the event of activated load supply, i.e., heating current flow with a value of I_1 = 500 A. In this case, Fig. 8b) indicates a significant increase in the interference signal level for the low frequency range up to 30 kHz. An interference signal in the higher frequency range, from 30 kHz to 150 kHz, decreases, as demonstrated in Fig. 8b) within the spectrum of interference signals impacting the environment, facilities and IESSs located therein.

Fig. 9 a) and b) show the unintentional electromagnetic field emission spectrum for the high frequency range, i.e., from 150 kHz to 30 MHz. For this frequency range, field emission both for electromagnetic field background for the environment and with active heating current consumption with a value of I_1 = 500 A, as seen in attached waveforms, decreases and does not exceed the values set out in the EN – 501215H standards (blue line in Fig. a and b).

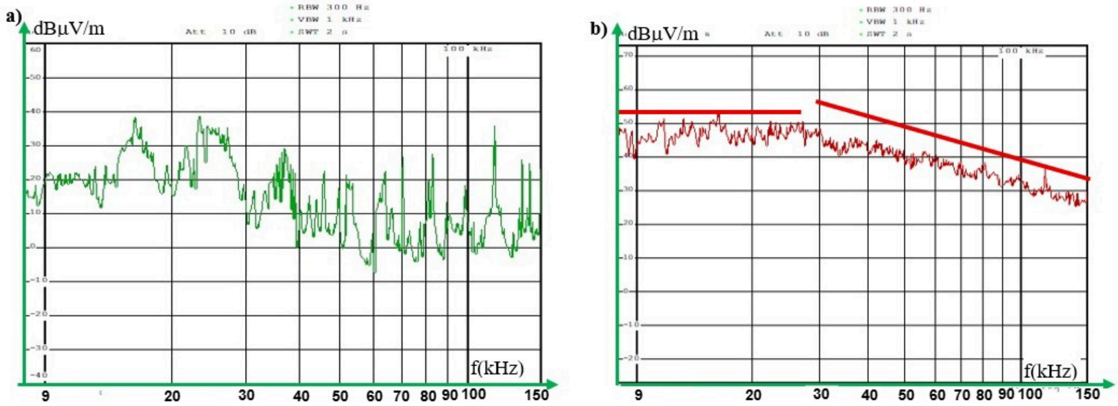

Figure 8. Unintentional electromagnetic field emission spectrum test results for the low frequency range (9 – 150) kHz, Fig. (7a) Electromagnetic field background for this frequency range, Fig. 8 (b) Electromagnetic field spectrum in the event of activated load supply, i.e., heating current flow with a value of I_1 = 500 A.

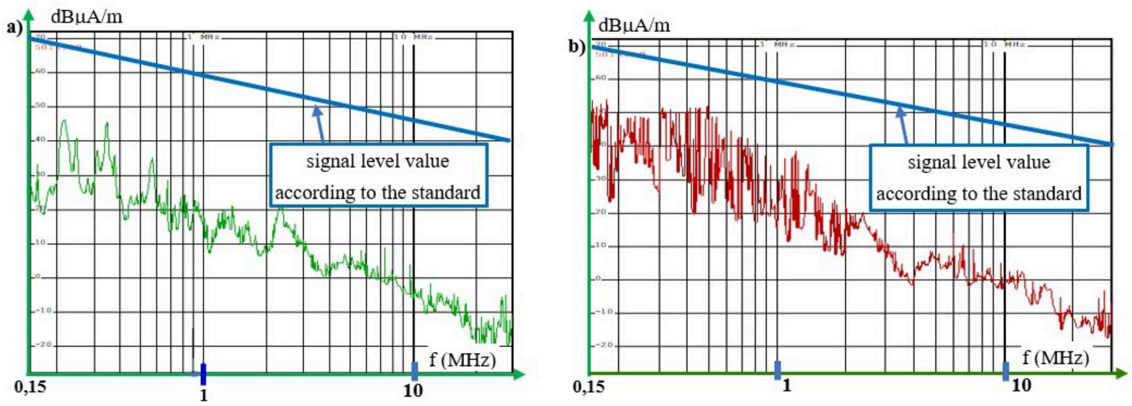

Figure 9. Unintentional electromagnetic field emission spectrum for the high frequency range, i.e., from 150 kHz to 30 MHz. For this frequency range, field emission both for electromagnetic field background for the environment and with active heating current consumption with a value of I_1 = 500 A, as seen in attached waveforms, decreases and does not exceed the values set out in the EN – 501215H standards (blue line in Fig. (a) and (b).

4. Research of the impact of radiated interference emission on the environment with IESSs operated – research results

Determining the impact of intentional and unintentional (stationary and non-stationary) electromagnetic radiation sources on an environment where an IESS is operated requires studying the effect of radiated interference emissions in the higher frequency range. The authors of this research paper executed such research in the vicinity of the Warszawa Zachodnia railway station in Warsaw. Interference signals in this range can propagate within a natural environment as electromagnetic waves over significant distances from their sources, and the nature of their impact on IESS elements, devices and modules is different than in the case of low frequencies – in the order of kHz. For this frequency range, interference signals propagate into the surrounding space and are proportional to the change rate of: current (di/dt) – inductive coupling, voltage (dU/dt) – capacitive coupling, electromagnetic field components (E – electric field strength, H – magnetic field strength). The impact of the aforementioned electromagnetic interference on IESSs is determined by, among others, the distance from interference sources, material composition, thickness, design, workmanships of reinforced ceilings (rebar grid size), building partition arrangement – e.g., walls in the protected facility or building openings – windows, doors, passageways, etc. The protected building's natural environment itself (e.g., temperature, humidity, pressure, etc.) also affects electromagnetic wave propagation within a confined space. Therefore, it is important to test the electromagnetic environment in the high frequency range and diagnose the distributions, characteristics and ranges of unintentional radiation sources in relation to IESS elements and devices.

Fig. 10 a, b, c and d show electromagnetic field background in the environment and building with operated IESSs. When measuring electromagnetic field background for this frequency range, all radiation sources should be deactivated for a given natural environment. The figure shows field background for various electromagnetic field frequency ranges and V and H vector polarisation. A red line marks permissible radiated interference emission values set out in the EN 50121-2 standard and specific areas mark cases of these values being exceeded.

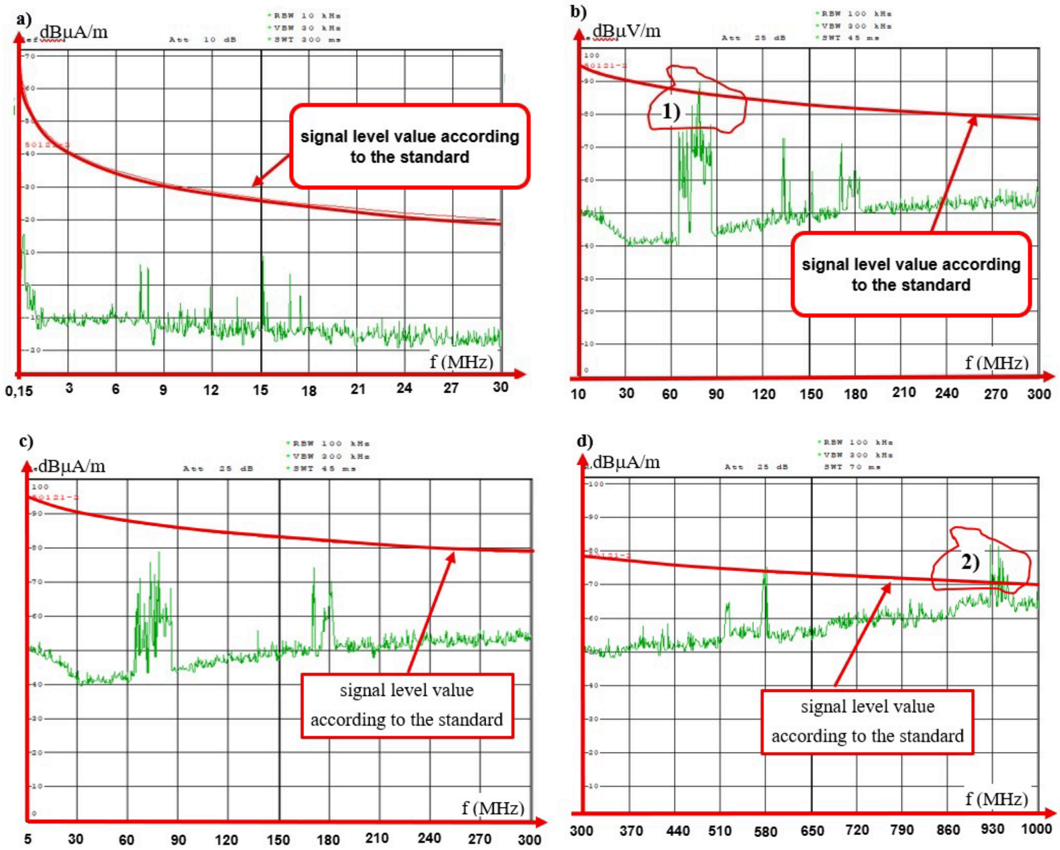

Figure 10. Electromagnetic field background in the environment and building with operated IESS, for different frequency ranges, and V and H polarisations, (a) electromagnetic field background spectrum for a frequency band from 150 kHz to 30 MHz, electromagnetic field component vector, H polarisation, (b) electromagnetic field background spectrum for a frequency band from 30 MHz to 300 MHz, V polarisation, (c) electromagnetic field background spectrum for a frequency band from 30 MHz to 300 MHz, electromagnetic field component vector, H polarisation, (d) electromagnetic field background spectrum for a frequency band from 300 MHz to 1 GHz, electromagnetic field component vector, H polarisation , 1,2 – areas of exceeded standard-specified interference emission values for this frequency range.

Fig. 11 illustrates an electromagnetic interference emission spectrum generated within an environment with operated IESS, with trains running on a railway track and all permissible interference sources being active. The spectrum covers a frequency range from 300 MHz to 1 GHz, for the V polarisation vector. Permissible standard values and areas 1 and 2, with exceeded permissible interference signals are colour-coded in the graph.

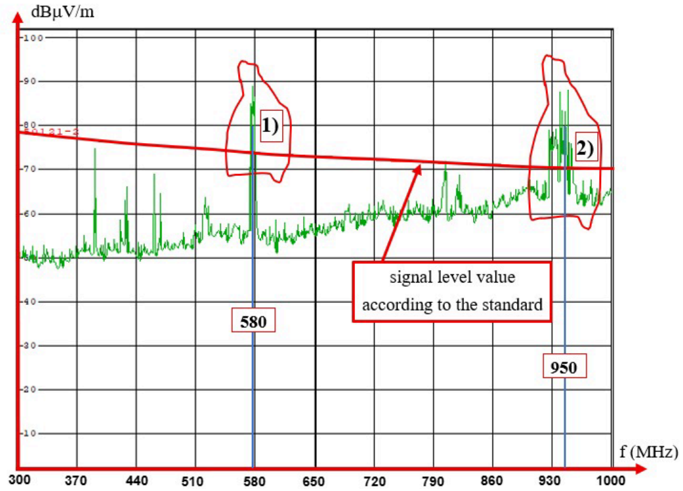

Figure 11. Electromagnetic interference emission spectrum generated within an environment with operated IESS, with trains running on a railway track and all permissible interference sources being active, frequency range from 300 MHz to 1 GHz; V polarisation; exceeded permissible interference signals are colour-coded.

Graphs 5 to 11 show electromagnetic field spectra and backgrounds for a natural environment with operated IESS. The presented spectra of the background and an electromagnetic environment with functioning security systems indicate that permissible standards for radiated interference, as well as electric and magnetic field component values are exceeded. Table 6 contains a summary of measurement result, however, only for exceeded values that apply to a specific environment. The impact of an electromagnetic field within the aforementioned frequency range on the IESS operation process should be studied separately, since electromagnetic interference propagating in a given environment penetrate ('attack') individual IESS elements, devices and modules. Low frequency interference propagates directly through conduction, most often over power supply, detection or transmission lines and circuits, usually hooked-up to an alarm control unit (ACU). In this case, the application of safeguards on such lines and circuits, in the form of filters with specific attenuation bands or anti-destructive components (varistor) is favourable in terms of an ACU. However, exceeding permissible interference signal values already at a given point on IESS detection lines may lead to incorrect operation of, e.g., a sensor. In such a case, the interference signal forces, e.g., a sensor from the detection state to a state of alarming or unfitness in the event of a high interference signal amplitude when there are local safeguards on detection lines or circuits – mostly on detectors or ACU input (connection point). In the case of emissions of interfering (distorting) signals in the high frequency range – above 30 MHz – the radiated electromagnetic field directly penetrates the structures of electronic modules, devices, and elements, as well as the ACUs themselves. In such a case, signal, supply or signal processing paths on the PCBs of sensors, modules, devices or ACUs themselves are interference receiving antennas. The electromagnetic field can induce interference signals also on detection loops or circuits (e.g., signal cables). In such a case, interference signals propagate concurrently with utility signals and are not automatically detected in the ACU, which may lead to changes in IESS technical status – transition from a state of monitoring to alarm or, e.g., unfitness – partial failure of only the detection line and connected sensors or the entire ACU.

Table 6. A summary of measurement results only for exceeded standard values applicable to a given electromagnetic environment, background and interference, low and high frequencies for conducted and radiated signals.

Electromagnetic field frequency range	Electromagnetic field background	Interference occurring within an environment after activating interference sources – level
(30 – 230) MHz – Fig. 6	standard not exceeded	antenna V, **area 1**, max. signal value 60 dBµV/m, for f = (30 – 38) MHz; antenna H, **area 2**, max. signal value 64 dB dBµV/m, for f = (30 – 74) MHz; antenna H, **area 3**, max. signal value 56 dB dBµV/m, for f = 187 MHz
(30 – 300) MHz – Fig. 9 b)	antenna V, **area 1**, max. signal value 90 dBµV/m, for f = 98 MHz;	standard not exceeded
(300 – 1000) MHz – Fig. 9 d)	antenna H, **area 2**, max. signal value 80 dBµA/m, for f = (930 – 954) MHz	standard not exceeded
(300 – 1000) MHz – Fig. 10	standard not exceeded	antenna V, **area 1**, max. signal value 90 dBµV/m, for f = 580 MHz; antenna V, **area 2**, max. signal value 88 dBµV/m, for f = (925 – 955) MHz

The measurement session regarding the impact of electromagnetic interference on selected electronic security systems was conducted on the experimental track of the Railway Institute in Warsaw. This was motivated by the fact that obtaining a permit for studies on an actual railway track (route) is time-consuming, difficult and required different technical approvals from various companies. Measurements of individual E, H electromagnetic field components were executed as per applicable legislation on field studies in a generally available natural environment. The tests were completed during the day, with no precipitation and fog, good visibility and a positive temperature of +18 ^{0}C. A locomotive was travelling at a speed of V = 50 km/h (± 10%) of that value. Higher speeds of the rail vehicle would require considering additional electromagnetic interference generated also by the contacts of the pantograph connecting electric receivers of the locomotive and the railway traction. The railway traction was supplied with a rated voltage of 3 kV. The traction substation was located approximately 3 km from the measuring points distributed along the railway track. Such a measurement distance was decided because there was no impact of electromagnetic interference generated by the traction substation itself, supplied by alternating voltage from an industrial grid – 110 kV (also no impact on the environment and measurement by interference generated by the cables of supply phases L1, L2, L3). When passing along the railway route – test track, all of the electric locomotive's current consumers (including heating) were active and set to maximum consumption of current from the contact line. A locomotive travelling along a railway track was not loaded with, e.g., freight cars with cargo or passenger cars (lower consumption of current from the contact line, but the test track offers such technical features). The tests addressing the impact of electromagnetic interference on ESS were determined for crucial security systems, i.e., fire alarm systems responsible for life, health, environment and accumulated property.

In the course of the experimental studies, the impact of interference generated over a vast railway area was tested using a fire alarm control panel (FACP). In the event of a rail vehicle passing by an area with an installed FAS, the response of the entire security system to unintentionally generated interference was observed. If, at this time, a detector within a detection circuit (line) reports a change of its technical state (transition type: monitoring – alarm, monitoring – failure), this was caused by exceeding a permissible interference level 'tolerated' by a given component. A transition like monitoring – alarm was always confirmed in a FAS by the operators, who checked for an actual fire. Whereas, the information on which element was 'triggered' within the FAS was displayed on the FACP LCD panel as a message – state change of detector C1245 (monitoring – alarm). In the case of most studied FASs, the elements most susceptible to electromagnetic interference were detectors located nearest to the source of interfering signals – i.e., the locomotive.

5. Operation process models for electronic security systems employed for building protection

IESS is tasked with ensuring security in protected buildings or over vast areas. Fig. 12 contains a diagram-based presentation of two security systems – FAS and IDS, employed for protection in a PF building. Individual detection lines of acoustic and optical signalling devices, sensors and manual call points used within the FAS, due to an unfitness related to a short-circuit or open-circuit, may contains a maximum of up to 30 elements only. An alarm is triggered in the event of security systems detecting a threat (e.g., fire, intrusion, robbery, etc.) within the protected PF facility. Simultaneously, an alarm and failure signal is sent via two independent ICT channels to an alarm receiving centre (ARC). The frequencies of these signals differ depending on the ESS, i.e., , f_{21},f_{22} – IDS alarm and failure signal transmitter frequencies, f_{11},f_{12} – FAS alarm and failure signal transmitter frequencies. The IESSs employed in the building are sufficient to ensure an appropriate level of security in relation to the protected property. Information on a state of unfitness or alarms is utilised in the building with 24/7 surveillance over the operation of these systems. At the same time, information on alarms and states of unfitness is sent to an ARC. A service crew and a response team are located in a remote receiving centre, ready to take immediate action in the protected facility. A fire alarm signal is automatically sent to the State Fire Service (SFS). Because of the protected facility (small size), FAS detection line accommodate up to 30 elements. FAS detection lines in each element - S_1,S_2,…,S_n, C_1,C_2,…,C_n, and O_1,O_2,…,O_n (connection joints, recovery of these elements) are fitted with short-circuit protections – Fig. 13.

Electromagnetic interference present within a railway environment always impact electronic security systems (ESS) over two frequency ranges. The first one covers low frequencies up to 30 MHz. The interference propagates particularly in power supply circuits, and detection lines and circuits as conducted interference. The second frequency range, above 30 MHz, includes radiated interference proportional to the rate of changes in the voltage or current flowing within ESS circuits, but also to the electromagnetic wave energy. This division was taken into account in the model demonstrating the impact of electromagnetic interference on a selected ESS, an FAS in this case, by introducing two coefficients: μ - responsible for the low frequency range, while coefficient Γ is the high frequency range. In the absence of interference within a natural environment, so-called *laboratory environment*, the coefficients are μ = 0, Γ = 0, respectively. If only low-frequency interference occurs, then μ ≠ 0, while Γ = 0. In the presence of high-frequency interference, above 30 MHz, then μ = 0, while Γ ≠ 0. The μ and Γ coefficients directly impact the λ failure intensity of electronic components making up detectors, devices, modules, manual call points, acoustic and optical signalling devices, etc. The impact of the μ and Γ coefficients is proportional: for the low frequency range, these are, e.g., interference current and voltage on common earthing impedance, whereas for the high frequency range, it is proportional to the voltage (current) change rate over time – capacitive and inductive coupling in ESS circuits or to signal strength – electromagnetic wave. Increasing the level of interference both in the low and high frequency range leads to elevated failure intensity λ of electronic elements through, e.g, additional voltages or current inducing within the structure itself or on the printed circuit boards of ESS devices. The greater the electromagnetic interference level, e.g., amplitude of voltage, current or signal strength [W/m^2] the higher the unfitness probability in the components or the detectors themselves (which contain many electronic elements on the printed circuit board). ESS components and devices contain a large number of active and passive elements exhibiting various reserves of resistance to electromagnetic, electric, environmental, thermal and mechanical interference, generated intentionally or unintentionally. These resistances are often subject to change under different environmental factors, e.g., temperature, humidity, electromagnetic interference, pressure, etc. Therefore, in general, the X resistance reserve for all ESS elements, modules or devices can be expressed as (1):

$$X = \sum_{i=0}^{k_z} X_i \quad (1)$$

where: Xi – resistance reserve for individual ESS components (e.g., transistors, resistors, integrated circuits, microprocessors, etc.).

Taking into account resistance to various external and internal impacts, natural or artificial (intentional or unintentional), the failure intensity λ(t) for an ESS can be determined via the expression (2)):

$$\lambda(t) = \frac{\delta F(t)}{\delta X_Z} \cdot \sum_{i=0}^{k_z} \frac{\delta X_Z}{\delta t} + \frac{\delta F(t)}{\delta X_m} \cdot \sum_{i=0}^{k_z} \frac{\delta X_m}{\delta t} + \frac{\delta F(t)}{\delta X_E} \cdot \sum_{i=0}^{k_z} \frac{\delta X_E}{\delta} + \frac{\delta F(t)}{\delta X_C} \cdot \sum_{i=0}^{k_z} \frac{\delta X_C}{\delta t} \quad (2)$$

Where, accordingly, as a mathematical relationship (2) addressing failure intensity λ(t) for a given ESS, the functions found within the formula determine the following, e.g., changes: σX/σt - resistance reserve change rate of an element(s) under the impact of internal degradation-related processes, (σXZ)/σt - resistance reserve change rate of an element(s) under the impact of mechanical, electrical, environmental and other interference, while σF(t)/σXZ determines the unreliability change rate of ESS components due to changes in their electrical (overvoltages, decays, dips, etc.), mechanical (vibrations, shocks, etc.), chemical and other resistances, whereas σF(t)/σXZ determines the change rate in the unreliability of ESS components under the impact of electromagnetic interference in various frequency ranges.

In the available source literature, the failure intensity change λ(t) is sometimes determined also using the coefficient k_λ. This coefficient is employed to analyse the impact of, e.g., atmospheric environment (including interference) using ESS data This coefficient indicates a numerical value of the many times the actual failure intensity λ_{rz} under given ESS operating conditions (e.g., temperature, humidity, pressure, electromagnetic environment, etc.) is higher or lower compared to the rated value determined under so-called *laboratory conditions*, where the aforementioned parameters are stabilised and constant. Then, the same failure intensity λ(t) value can be expressed as (3).

$$k_\lambda = \frac{\lambda_{rz}}{\lambda} \quad (3)$$

where: k_λ - ESS component failure intensity coefficient, λ_{rz}- actual ESS component failure intensity, λ- ESS component failure intensity under laboratory conditions.

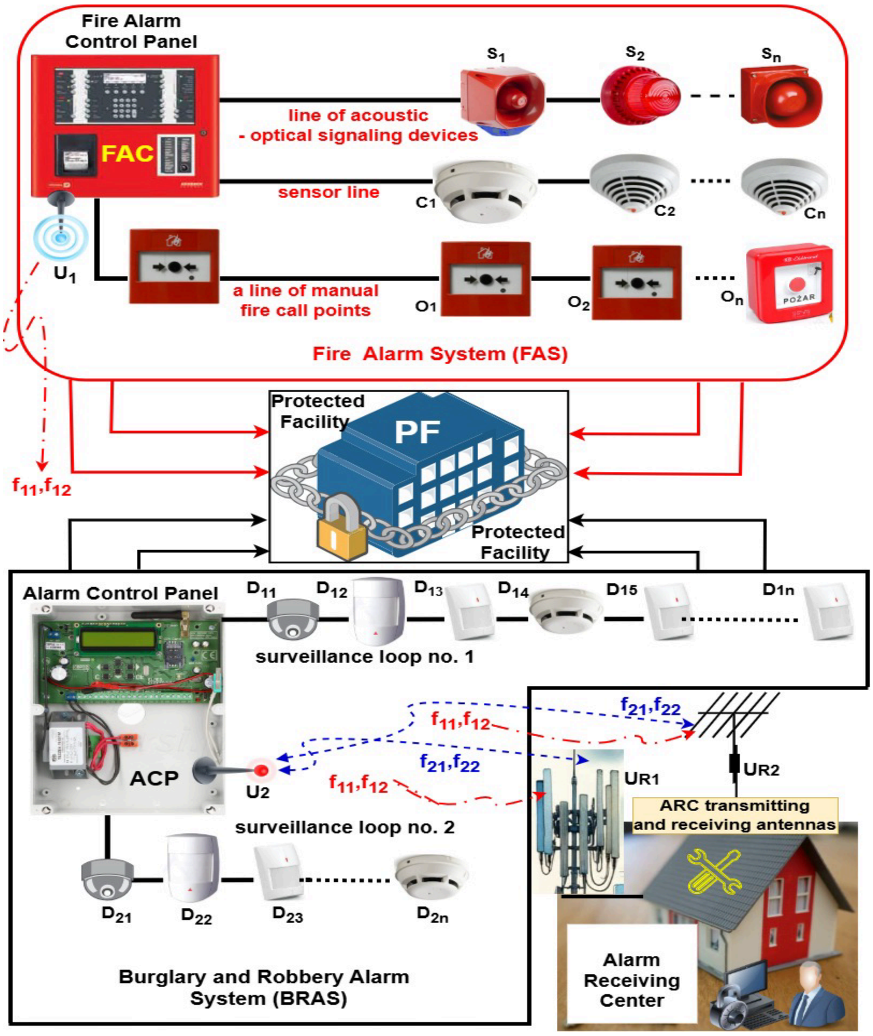

Figure 12. ESS operated in a protected facility, where: f_{11},f_{12} – FAS alarm and failure signal transmission equipment frequencies, f_{21},f_{22} – IDS alarm and failure signal transmission equipment frequencies, S_1,S_2,…,S_n – acoustic and optical signalling device detection line, C_1,C_2,…,C_n – sensor detection line, O_1,O_2,…,O_n – manual call point detection line, D_{11},D_{12},…,D_{1n} – IDS sensor transmission line No. 1, D_{21},D_{22},…,D_{2n} – IDS sensor transmission line No. 2, U_{R1},U_{R2} – ARC transceiver antennas, U_1,U_2 – ACP, FAS transceiver antennas.

Fig. 13 illustrates an expanded IESS employed to protect a facility classified as SCI. The IESS was equipped with two additional systems – CCTV and ACS. These two additional security systems are responsible also for internal and external traffic within the monitored facility. Moreover, CCTV also enables identifying and confirming alarms.

The following operation model assumptions regarding the entire fire alarm system were made in the paper. These are constant failure intensity λ and an exponential distribution of reliability probability. This is because each component, device, module, detector, etc. or the alarm control panel itself is subject to 'preliminary ageing' within a manufacturing plant. The authors of the paper conducted two site visits in FAS manufacturing plants, where they could familiarise themselves with the occurrence of this process during production first-hand. This is a crucial operation process for FAS components, associated with manufacturing itself, since it enables early identification and detection of various fault types – e.g., incorrect, so-called '*cold soldering*' of electronic elements, absence of connections or wireless signal transmission, short-circuits or open circuits in printed circuit boards, changes in the characteristic resistance of detectors, etc. FAS components, selected based on statistics are additionally placed in an environmental chamber and subjected to climatic exposure – e.g., change in temperature or humidity for FAS detectors. After initial ageing at the plant, all component are additionally inspected at the assembly line and then released to sales.

Classic detectors or other FAS elements do not usually include technical solutions of sensors with on-line continuous measuring of 'electromagnetic smog' and taking its level into account when generating alarm signals, in particular. So-called *linear smoke detectors* or aspirating systems are employed in the event of strong electromagnetic interference in monitored spaces or rooms – e.g., switching stations, server rooms, etc. These are detectors that detect characteristic fire values insensitive to present electromagnetic interference since they are fitted with appropriate technical solutions. For a linear smoke detector in the form of – an infrared-range electromagnetic radiation receiver and transmitter, appropriately shielded for a split or combined detector. FAS aspirating system in particular are suitable for operation in rooms or spaces with high levels of interference signals. Such a detector is equipped with a plastic tube with boreholes (each hole is a detector) routed to a room with electromagnetic interference. Whereas the decision-making electronic element (alarm-monitoring, failure), as well as the aspirating system – fan is placed in another room, where the interference level (electromagnetic environment) is not distorted.

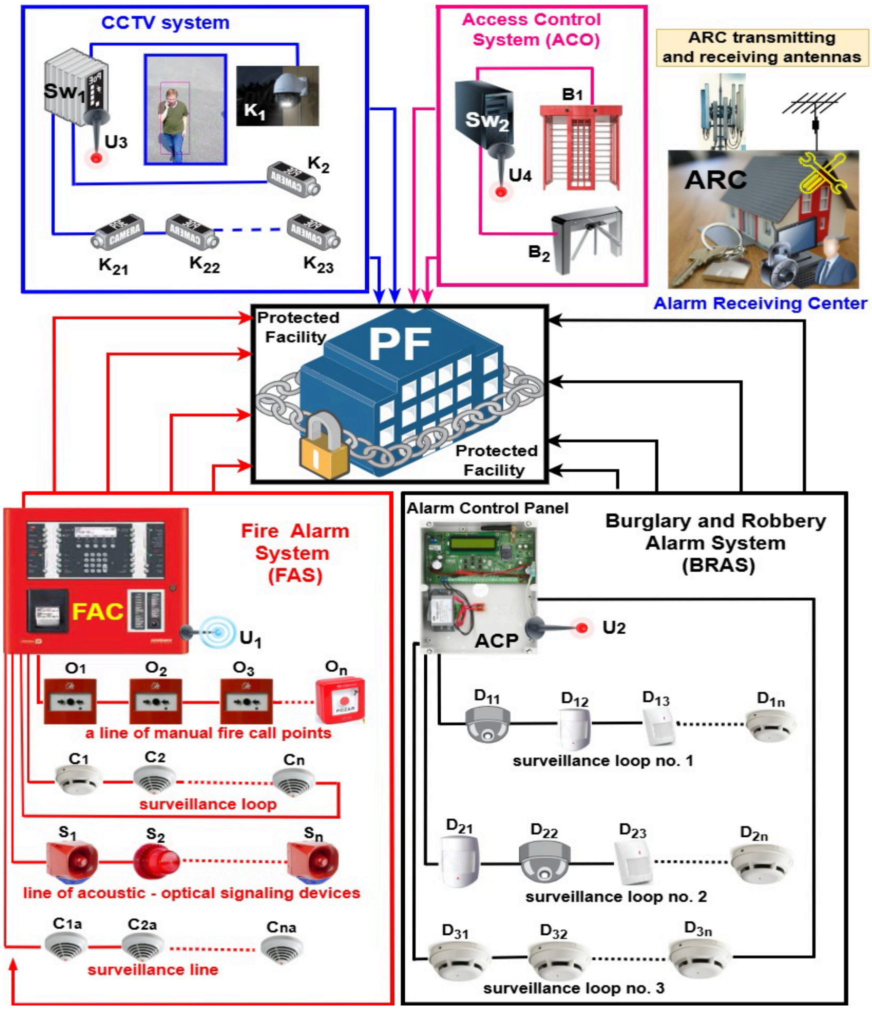

Figure 13. IESS operated in a SCI facility (certain designations correspond to Fig. 12) were, in relation to infrastructure protection, equipped with: FAS – detection circuit with sensors $C_1, C_2, \ldots, C_n$ and detection circuit with sensors $C_{1a}, C_{2a}, \ldots, C_{na}$; IDS used a detection circuit for a line of sensors $D_{31}, D_{32}, \ldots, D_{3n}$, U_1, U_2, U_3, U_4, alarm and failure signal transmitters and receivers for ARC, S_{w1}, S_{w2} – event loggers (servers) within protected facilities, respectively for CCTV and ACS, $K_1, K_2, K_{21}, K_{22}, \ldots, K_{23}$ – cameras for event observation and recording in the facility, B_1, B_2 – tripods (entry and exit gates) for the ACS systems; Fig. 5 does not show wireless and wired connections U_1, U_2, U_3, U_4 with ARS transceiver antennas due to the legibility of the entire illustrations; the task of all IESSs is to ensure security in a SCI buildings, as shown via lines assigned to consecutive ESSs.

Fig. 14 demonstrates the operation process model for an ESS employed to ensure an appropriate security level in the building, as in Fig. 12. Due to the property accumulated and stored inside rooms, only two ESSs – FACP and IDS – were employed in this case. Electromagnetic interference in two different frequency ranges, which impact the operation process were taken into account separately for each of the distinguished sub-ranges. Low frequencies were marked as μ, while high frequencies as Γ. The propagation nature of electromagnetic interference impacting ESSs within these two frequency ranges should be considered independently. Low frequency interference always propagates along power supply lines, transmission lines of sensors or telecommunication lines, as well as detection lines in FAS. Protections against such interference include filters, stabilisers, anti-destructive elements (e.g., varistors) in the ACU itself or on the detection line input. It is different in the case of high frequency radiated interference propagation. The interference signal that reaches individual, spatially arranged ESS elements in a building depends on, e.g., interference source location, frequency range of such a transmitter or construction obstacles along the propagation path of such electromagnetic interference. It also includes the degree of exposure of a given ESS element – sensor, module, etc. to electromagnetic waves, taking into account the propagation nature of such interference. Therefore, the failure intensity λ for individual elements should take into account two different interference impact factors: μ – low frequency range, Γ – high frequency range as shown in Fig. 14 – designations $(\mu,\Gamma)\bullet\lambda_{ZBa1},\ldots,(\mu,\Gamma)\bullet\lambda_{ZBa2}$. The interference phenomena above also impact μ recovery intensity of the ESS operation process as shown in the operation process graph – e.g. $(\mu,\Gamma)\bullet\mu_{ZBa1}, \ldots, (\mu,\Gamma)\bullet\mu_{ZBa2}$. The ESS operation graph does not include the reliability for the process of transmitting information on a state of alarm, failure or monitoring outside of the protected facility to the ARC. This is due to the presence of a hot reserve in the transmission of these signals to ARC or SFS, at two, always different, frequencies f_{11}, f_{12}, f_{21}, f_{22} – Fig. 12. Transmitted alarm signals, due to the digital modules, coding and simultaneous encryption employed, are resistant to interference within a given environment that is independent of the frequency range for these unwanted sources.

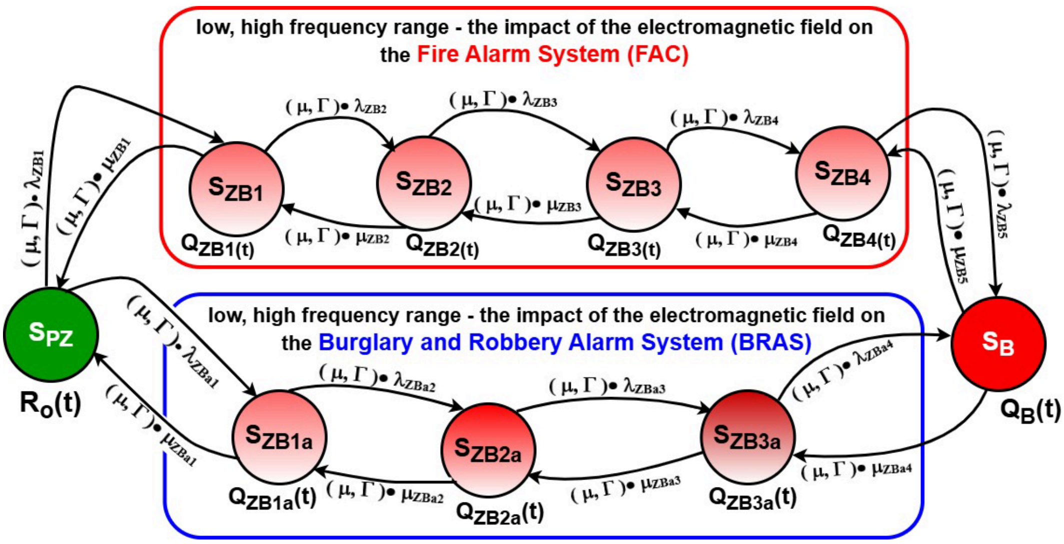

Figure 14. Operation process model for an ESS employed to ensure an appropriate security level in the protected building, where: (μ,Γ) interference signal low and high frequency range, respectively, $(\mu,\Gamma)\bullet\lambda_{ZBa1}, \ldots, (\mu,\Gamma)\bullet\lambda_{ZBa2}$ – impact of the interference in these frequency ranges on failure intensity λ for individual ESS elements, impact of low and high frequency range interference on ESS recovery intensity μ – e.g., $(\mu,\Gamma)\bullet\mu_{ZBa1}, \ldots, (\mu,\Gamma)\bullet\mu_{ZBa2}$ (assumption: different type of failure in ESS elements and modules exposed to interference in frequency rangesμ, Γ).

Fault isolators (FI) are employed virtually in every component, device and module within the detection lines and circuits of fire alarm systems (FAS). The task of Fis on detection lines and circuits hooked-up to fire alarm control panel (FACP) is responding to potential short-circuits within these circuits. In such a case, the following parameters of these electric circuits change in FAS detection circuits or lines: Z_l=0, supply voltage U_{zas}=0, supply current I_{zas}=max. The causes behind a short-circuit in FAS detection lines or circuits include, e.g., overvoltages within a power supply grid, but also electromagnetic interference propagating within the nearest environment surrounding a given system. The nature of such interference may be neutral (e.g., lightning pulses) or artificial, unintentional nature, resulting from e.g., locomotive moving along a railway track (non-stationary interference sources) or may be stationary (radio and TV station transmitters, radars, mobile telephony transmitters, etc.). In the event on differences in rated supply parameters of detection circuits, Fis isolate a damaged circuit section and its power supply from two terminals (1, 2) connected to a fire alarm control panel.

Fire alarm systems operated over a vast railway area function within a distorted electromagnetic environment. Ten different FASs of varying functional structure (the number of detection lines and circuits, detectors, etc.) were operationally studied. Numerical unfitness values for these ten FASs operated in railway facilities were determined based on test lasting a whole year. This was demonstrated in Table 7.

Table 7. List of unfitness states for ten studied FASs operated in railway facilities.

No. of facility with an operated FAS	Operational disturbances of a detection line or circuit	Detection line or circuit ground fault (short-circuit)	Interrupted detection line (open circuit)	No alarm control panel printer paper	Activated fault isolator in a detector, module (line short-circuit)	No primary 230 V power supply, back-up power supply
Facility 1	87	6	13	2	27	13
Facility 2	58	-	3	1	15	15
Facility 3	89	14	8	2	12	10
Facility 4	43	-	24	1	-	19
Facility 5	56	9	16	1	-	-
Facility 6	35	-	23	2	-	11
Facility 7	64	10	13	2	12	8
Facility 8	43	-	26	1	-	-
Facility 9	103	6	13	1	20	-
Facility 10	66	-	5	3	5	15

For the purposes of determining FAS reliability, the authors also studied different repair times for sample failures, demonstrated accordingly in Tab. 7. Fig. 15 illustrates FAS failures of the 'line/circuit interference' type for ten studies FASs. The following values were obtained for failures of this type: mean repair time: 4 h 28 min., minimum repair time: 5 min., maximum repair time: 9 h 38 min., and repair time standard deviation: 2 h 38 min.

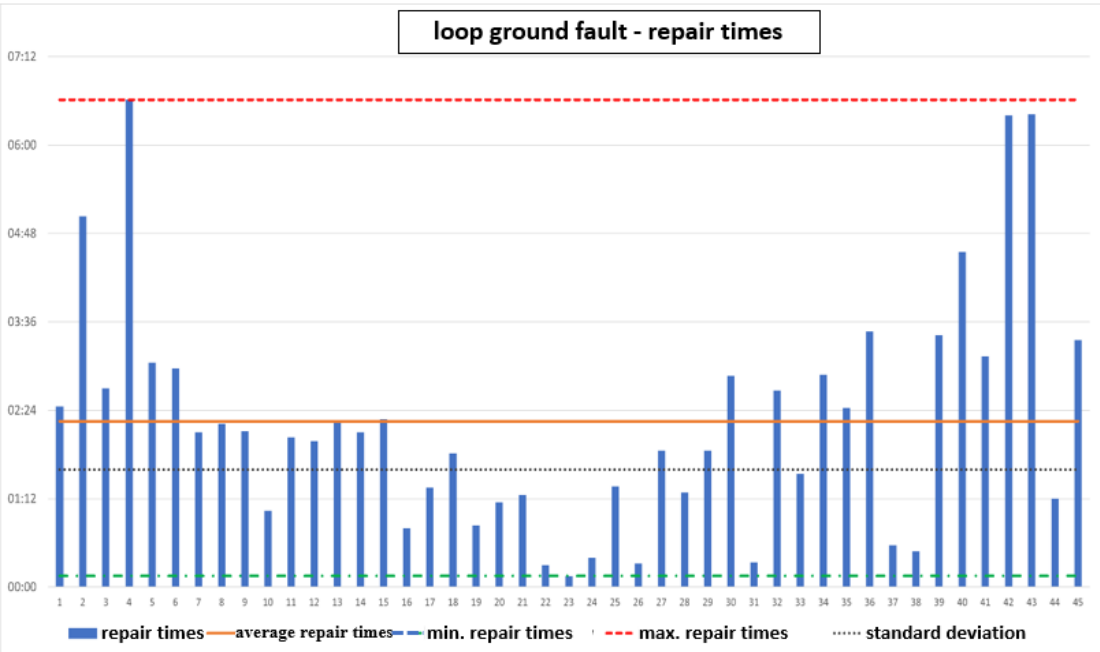

Figure 15. Repair times for the "circuit ground fault" failure type for ten studied FASs operated over a vast railway area. The following recovery times were obtained for such failures in ten studied FASs: mean repair time: 2 h 15 min., minimum repair time: 9 min., maximum repair time: 6 h 37 min., and repair time standard deviation: 1 h 35 min.

The FASs were operated within a given electromagnetic environment, during traction vehicle traffic on a railway track.

Individual FAS components, detectors, devices or modules do not have built-in sensors reporting whether a permissible electromagnetic interference level is exceeded. The application of such solutions, e.g., in detectors, would constitute an additional feature, highly desirable according to the officers of the State Fire Service. However, currently applicable legislation, which is rigorously observed in Poland, does not provide for such technical solutions. The authors came upon only one such technical solution, in a detector of an intrusion detection system, where the information on exceeding a permissible electromagnetic interference level was locally indicated (LED of the detector), with additional notification sent to an alarm control panel. The impact of electromagnetic interference within the considered model of an FAS operated over a vast railway area was approached ‘globally’. The authors did not take the electromagnetic field impact on individual security system components during, e.g, the passage of a rail vehicle. Information on the occurrence of a failure or a triggered alarm caused by electromagnetic interference at a given moment was received by a fire alarm control panel. The physics of electromagnetic impact on electronic systems is that it treats all components equally. An electromagnetic field is not selective, since it ‘attacks’ all components simultaneously with the same intensity (e.g., force). Upon such an incident, individual FAS components exhibiting the least resistance and highest susceptibility to electromagnetic interference within a given environment transit from a state of fitness to a state of unfitness or alarm. Determining, which FAS component was treated by an electromagnetic field this way requires conducting separate, time-consuming tests covering selected elements, since it necessitates considering different frequency range of interfering signals, a given operating configuration, location of such an element within the space where a wave propagates, shielding properties of the walls, etc.

The system shown in Fig. 14 can be described by the following Chapman–Kolmogorov equations:

$$
\begin{aligned}
R_0'(t) &= -\mu\Gamma_{\lambda ZB1}\cdot\lambda_{ZB1}\cdot R_0(t) + \mu\Gamma_{\mu ZB1}\cdot\mu_{ZB1}\cdot Q_{ZB1}(t) - \mu\Gamma_{\lambda ZBa1}\cdot\lambda_{ZBa1}\cdot R_0(t) + \mu\Gamma_{\mu ZBa1}\cdot\mu_{ZBa1}\cdot Q_{ZB1a}(t)\\
Q_{ZB1}'(t) &= \mu\Gamma_{\lambda ZB1}\cdot\lambda_{ZB1}\cdot R_0(t) - \mu\Gamma_{\mu ZB1}\cdot\mu_{ZB1}\cdot Q_{ZB1}(t) - \mu\Gamma_{\lambda ZB2}\cdot\lambda_{ZB2}\cdot Q_{ZB1}(t) + \mu\Gamma_{\mu ZB2}\cdot\mu_{ZB2}\cdot Q_{ZB2}(t)\\
Q_{ZB2}'(t) &= \mu\Gamma_{\lambda ZB2}\cdot\lambda_{ZB2}\cdot Q_{ZB1}(t) - \mu\Gamma_{\mu ZB2}\cdot\mu_{ZB2}\cdot Q_{ZB2}(t) - \mu\Gamma_{\lambda ZB3}\cdot\lambda_{ZB3}\cdot Q_{ZB2}(t) + \mu\Gamma_{\mu ZB3}\cdot\mu_{ZB3}\cdot Q_{ZB3}(t)\\
Q_{ZB3}'(t) &= \mu\Gamma_{\lambda ZB3}\cdot\lambda_{ZB3}\cdot Q_{ZB2}(t) - \mu\Gamma_{\mu ZB3}\cdot\mu_{ZB3}\cdot Q_{ZB3}(t) - \mu\Gamma_{\lambda ZB4}\cdot\lambda_{ZB4}\cdot Q_{ZB3}(t) + \mu\Gamma_{\mu ZB4}\cdot\mu_{ZB4}\cdot Q_{ZB4}(t)\\
Q_{ZB4}'(t) &= \mu\Gamma_{\lambda ZB4}\cdot\lambda_{ZB4}\cdot Q_{ZB3}(t) - \mu\Gamma_{\mu ZB4}\cdot\mu_{ZB4}\cdot Q_{ZB4}(t) - \mu\Gamma_{\lambda ZB5}\cdot\lambda_{ZB5}\cdot Q_{ZB4}(t) + \mu\Gamma_{\mu ZB5}\cdot\mu_{ZB5}\cdot Q_{B}(t)\\
Q_{ZB1a}'(t) &= \mu\Gamma_{\lambda ZBa1}\cdot\lambda_{ZBa1}\cdot R_0(t) - \mu\Gamma_{\mu ZBa1}\cdot\mu_{ZBa1}\cdot Q_{ZB1a}(t) - \mu\Gamma_{\lambda ZBa2}\cdot\lambda_{ZBa2}\cdot Q_{ZB1a}(t) + \mu\Gamma_{\mu ZBa2}\cdot\mu_{ZBa2}\cdot Q_{ZB2a}(t)\\
Q_{ZB2}'(t) &= \mu\Gamma_{\lambda ZBa2}\cdot\lambda_{ZBa2}\cdot Q_{ZB1a}(t) - \mu\Gamma_{\mu ZBa2}\cdot\mu_{ZBa2}\cdot Q_{ZB2a}(t) - \mu\Gamma_{\lambda ZBa3}\cdot\lambda_{ZBa3}\cdot Q_{ZB2a}(t) + \mu\Gamma_{\mu ZBa3}\cdot\mu_{ZBa3}\cdot Q_{ZB3a}(t)\\
Q_{ZB3}'(t) &= \mu\Gamma_{\lambda ZBa3}\cdot\lambda_{ZBa3}\cdot Q_{ZB2a}(t) - \mu\Gamma_{\mu ZBa3}\cdot\mu_{ZBa3}\cdot Q_{ZB3a}(t) - \mu\Gamma_{\lambda ZBa4}\cdot\lambda_{ZBa4}\cdot Q_{ZB3a}(t) + \mu\Gamma_{\mu ZBa4}\cdot\mu_{ZBa4}\cdot Q_{B}(t)\\
Q_{B}'(t) &= \mu\Gamma_{\lambda ZB5}\cdot\lambda_{ZB5}\cdot Q_{ZB4}(t) - \mu\Gamma_{\mu ZB5}\cdot\mu_{ZB5}\cdot Q_{B}(t) + \mu\Gamma_{\lambda ZBa4}\cdot\lambda_{ZBa4}\cdot Q_{ZB3a}(t) - \mu\Gamma_{\mu ZBa4}\cdot\mu_{ZBa4}\cdot Q_{B}(t)
\end{aligned}
\tag{4}
$$

Assuming the baseline conditions:

$$
\begin{gathered}
R_0(0) = 1\\
Q_{ZB1}(0) = Q_{ZB2}(0) = Q_{ZB3}(0) = Q_{ZB4}(0) = Q_{ZB1a}(0) = Q_{ZB2a}(0) = Q_{ZB3a}(0) = Q_B(0) = 0
\end{gathered}
\tag{5}
$$

and applying the Laplace transform, the following system of linear equations is obtained:

$$
\begin{aligned}
s\cdot R_0^*(s) - 1 &= -\mu\Gamma_{\lambda ZB1}\cdot\lambda_{ZB1}\cdot R_0^*(s) + \mu\Gamma_{\mu ZB1}\cdot\mu_{ZB1}\cdot Q_{ZB1}^*(s) - \mu\Gamma_{\lambda ZBa1}\cdot\lambda_{ZBa1}\cdot R_0^*(s) + \mu\Gamma_{\mu ZBa1}\cdot\mu_{ZBa1}\cdot Q_{ZB1a}^*(s)\\
s\cdot Q_{ZB1}^*(s) &= \mu\Gamma_{\lambda ZB1}\cdot\lambda_{ZB1}\cdot R_0^*(s) - \mu\Gamma_{\mu ZB1}\cdot\mu_{ZB1}\cdot Q_{ZB1}^*(s) - \mu\Gamma_{\lambda ZB2}\cdot\lambda_{ZB2}\cdot Q_{ZB1}^*(s) + \mu\Gamma_{\mu ZB2}\cdot\mu_{ZB2}\cdot Q_{ZB2}^*(s)\\
s\cdot Q_{ZB2}^*(s) &= \mu\Gamma_{\lambda ZB2}\cdot\lambda_{ZB2}\cdot Q_{ZB1}^*(s) - \mu\Gamma_{\mu ZB2}\cdot\mu_{ZB2}\cdot Q_{ZB2}^*(s) - \mu\Gamma_{\lambda ZB3}\cdot\lambda_{ZB3}\cdot Q_{ZB2}^*(s) + \mu\Gamma_{\mu ZB3}\cdot\mu_{ZB3}\cdot Q_{ZB3}^*(s)\\
s\cdot Q_{ZB3}^*(s) &= \mu\Gamma_{\lambda ZB3}\cdot\lambda_{ZB3}\cdot Q_{ZB2}^*(s) - \mu\Gamma_{\mu ZB3}\cdot\mu_{ZB3}\cdot Q_{ZB3}^*(s) - \mu\Gamma_{\lambda ZB4}\cdot\lambda_{ZB4}\cdot Q_{ZB3}^*(s) + \mu\Gamma_{\mu ZB4}\cdot\mu_{ZB4}\cdot Q_{ZB4}^*(s)\\
s\cdot Q_{ZB4}^*(s) &= \mu\Gamma_{\lambda ZB4}\cdot\lambda_{ZB4}\cdot Q_{ZB3}^*(s) - \mu\Gamma_{\mu ZB4}\cdot\mu_{ZB4}\cdot Q_{ZB4}^*(s) - \mu\Gamma_{\lambda ZB5}\cdot\lambda_{ZB5}\cdot Q_{ZB4}^*(s) + \mu\Gamma_{\mu ZB5}\cdot\mu_{ZB5}\cdot Q_{B}^*(s)\\
s\cdot Q_{ZB1a}^*(t) &= \mu\Gamma_{\lambda ZBa1}\cdot\lambda_{ZBa1}\cdot R_0^*(s) - \mu\Gamma_{\mu ZBa1}\cdot\mu_{ZBa1}\cdot Q_{ZB1a}^*(s) - \mu\Gamma_{\lambda ZBa2}\cdot\lambda_{ZBa2}\cdot Q_{ZB1a}^*(s) + \mu\Gamma_{\mu ZBa2}\cdot\mu_{ZBa2}\cdot Q_{ZB2a}^*(s)\\
s\cdot Q_{ZB2a}^*(t) &= \mu\Gamma_{\lambda ZBa2}\cdot\lambda_{ZBa2}\cdot Q_{ZB1a}^*(s) - \mu\Gamma_{\mu ZBa2}\cdot\mu_{ZBa2}\cdot Q_{ZB2a}^*(s) - \mu\Gamma_{\lambda ZBa3}\cdot\lambda_{ZBa3}\cdot Q_{ZB2a}^*(s) + \mu\Gamma_{\mu ZBa3}\cdot\mu_{ZBa3}\cdot Q_{ZB3a}^*(s)\\
s\cdot Q_{ZB3a}^*(t) &= \mu\Gamma_{\lambda ZBa3}\cdot\lambda_{ZBa3}\cdot Q_{ZB2a}^*(s) - \mu\Gamma_{\mu ZBa3}\cdot\mu_{ZBa3}\cdot Q_{ZB3a}^*(s) - \mu\Gamma_{\lambda ZBa4}\cdot\lambda_{ZBa4}\cdot Q_{ZB3a}^*(s) + \mu\Gamma_{\mu ZBa4}\cdot\mu_{ZBa4}\cdot Q_{B}^*(s)\\
s\cdot Q_{B}^*(s) &= \mu\Gamma_{\lambda ZB5}\cdot\lambda_{ZB5}\cdot Q_{ZB4}^*(s) - \mu\Gamma_{\mu ZB5}\cdot\mu_{ZB5}\cdot Q_{B}^*(s) + \mu\Gamma_{\lambda ZBa4}\cdot\lambda_{ZBa4}\cdot Q_{ZB3a}^*(s) - \mu\Gamma_{\mu ZBa4}\cdot\mu_{ZBa4}\cdot Q_{B}^*(s)
\end{aligned}
\tag{6}
$$

Further analysis was conducted assuming the following intensity values of transitions between distinguished states:

$$\lambda_{ZB1} = 0{,}000001[1/h],\ \lambda_{ZB2} = 0{,}0000008[1/h],\ \lambda_{ZB3} = 0{,}0000006[1/h],$$

$$\lambda_{ZB4} = 0{,}000000[1/h],\ \lambda_{ZB5} = 0{,}0000002[1/h],$$

$$\mu_{ZB1} = 0{,}1[1/h],\ \mu_{ZB2} = 0{,}1[1/h],\ \mu_{ZB3} = 0{,}1[1/h],\ \mu_{ZB4} = 0{,}1[1/h],\ \mu_{ZB5} = 0{,}1[1/h],$$

$$\lambda_{ZBa1} = 0{,}000001[1/h],\ \lambda_{ZBa2} = 0{,}0000008[1/h],$$

$$\lambda_{ZBa3} = 0{,}0000006[1/h],\ \lambda_{ZBa4} = 0{,}0000004[1/h],$$

$$\mu_{ZBa1} = 0{,}1[1/h],\ \mu_{ZBa2} = 0{,}1[1/h],\ \mu_{ZBa3} = 0{,}1[1/h],\ \mu_{ZBa4} = 0{,}1[1/h],$$

$$\mu\Gamma_{\lambda ZB1} = \mu\Gamma_{\lambda ZB2} = \mu\Gamma_{\lambda ZB3} = \mu\Gamma_{\lambda ZB4} = \mu\Gamma_{\lambda ZB5} = 0{,}5[1/h],$$

$$\mu\Gamma_{\mu ZB1} = \mu\Gamma_{\mu ZB2} = \mu\Gamma_{\mu ZB3} = \mu\Gamma_{\mu ZB4} = \mu\Gamma_{\mu ZB5} = 0{,}5[1/h]\,,$$
$$\mu\Gamma_{\lambda ZBa1} = \mu\Gamma_{\lambda ZBa2} = \mu\Gamma_{\lambda ZBa3} = \mu\Gamma_{\lambda ZBa4} = 0{,}5[1/h]\,,$$
$$\mu\Gamma_{\mu ZBa1} = \mu\Gamma_{\mu ZBa2} = \mu\Gamma_{\mu ZBa3} = \mu\Gamma_{\mu ZBa4} = 0{,}5[1/h].$$

Study duration was assumed at 1 year, i.e. $t = 8760[h]$.

Using the system of equations (6), the following is obtained for the above input values assumed for the simulation:

$$R_0(t) = -0.00480149 \cdot e^{-0.0503986 \cdot t} + 1.00001 \cdot e^{-3.1999 \cdot 10^{-17} \cdot t} - 0.00002548 \cdot e^{2.99999 \cdot 10^{-7} \cdot t} -$$
$$e^{(-0.0496478 - 0.000140314 \cdot i) \cdot t} \cdot \left((-0.024622 + 0.0306289 \cdot i) - (0.024622 + 0.0306289 \cdot i) \cdot e^{(0.000280627 \cdot i) \cdot t}\right) -$$
$$e^{(-0.0502452 - 0.000262675 \cdot i) \cdot t} \cdot \left((0.003544 - 0.00083095 \cdot i) + (0.003544 + 0.00083095 \cdot i) \cdot e^{(0.00052535 \cdot i) \cdot t}\right) -$$
$$e^{(-0.0499093 - 0.000321158 \cdot i) \cdot t} \cdot \left((0.0186669 + 0.0147119 \cdot i) + (0.0186669 - 0.0147119 \cdot i) \cdot e^{(0.000642315 \cdot i) \cdot t}\right)$$

The end result (for $\boldsymbol{t = 8760[h]}$) is: $\boldsymbol{R_O = 0{,}99998}$.

Fig. 16 contains a graphic representation of the $\boldsymbol{R_O(t)}$ function.

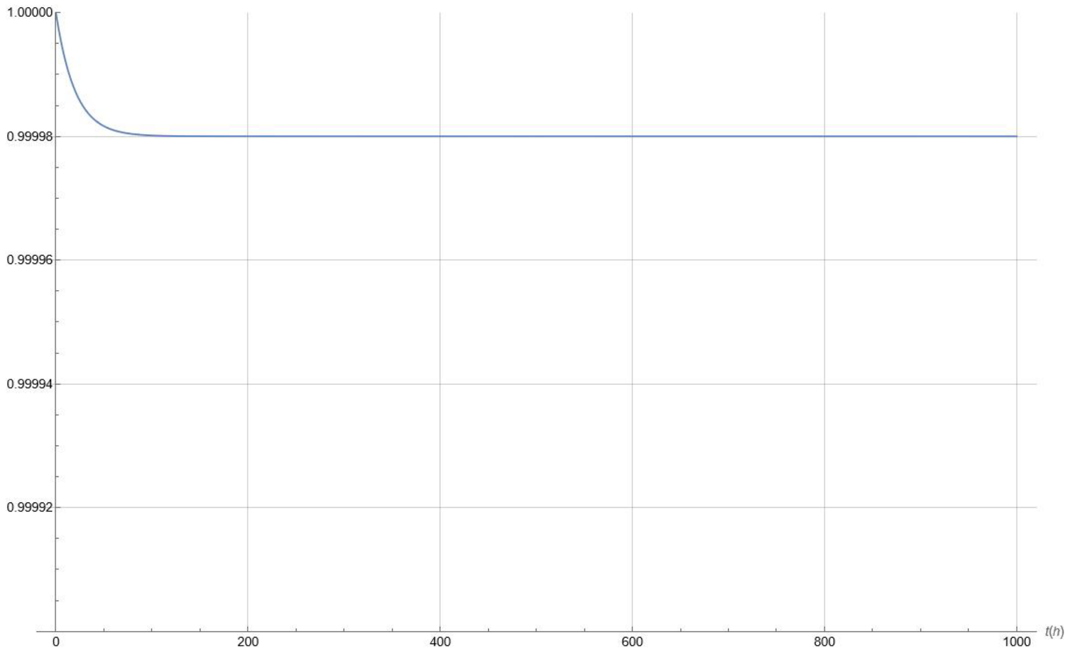

Figure 16. Graphic representation of the $\boldsymbol{R_O(t)}$ for the model illustrated in Fig. 14.

In order to check the correctness of the developed model, the disturbance impact coefficients were changed to the following value:

$$\mu\Gamma_{\lambda ZB1} = \mu\Gamma_{\lambda ZB2} = \mu\Gamma_{\lambda ZB3} = \mu\Gamma_{\lambda ZB4} = \mu\Gamma_{\lambda ZB5} = 0{,}75[1/h]$$
$$\mu\Gamma_{\lambda ZBa1} = \mu\Gamma_{\lambda ZBa2} = \mu\Gamma_{\lambda ZBa3} = \mu\Gamma_{\lambda ZBa4} = 0{,}75[1/h]$$

For the assumed values, calculations were performed again (including Laplace transformations), which enabled the determination of the function dependencies $R_O(t)$ - Fig. 17. The obtained graphical form confirms the correctness of the developed model.

Fig. 18 illustrates an operation model for an IESS used to protect facilities and vast areas classified as SCI. The IESS was additionally expanded with two security systems, CCTV and ACS. The FACP, due to the protection of the health and life of people residing in rooms, is a master security system. An FACP unfitness is locally monitored by a service crew, and additionally by persons in the ARC – Fig. 13. The local and remote service crews have a strict, predefined time to respond in relation to repairing the FACP and other security systems operated in facilities. IESS elements, devices and modules can be exposed to a total of three types of electromagnetic interference, namely:

(a) μ ≥ 0, Γ = 0 – low frequency interference appears in buildings and over a vast area;

(b) μ = 0, Γ ≥ 0 – only high frequency interference occurs in buildings and over a vast area; low frequency interference is attenuated by anti-destructive filters and elements located in the ACU;

(c) $\mu \geq 0, \Gamma \geq 0$ – interference in both ranges, low and high frequency, appears in buildings and across large areas.

The assumptions regarding the impact of electromagnetic interference adopted for the model in Fig. 14 apply also the the extended IESS demonstrated in Fig. 18.

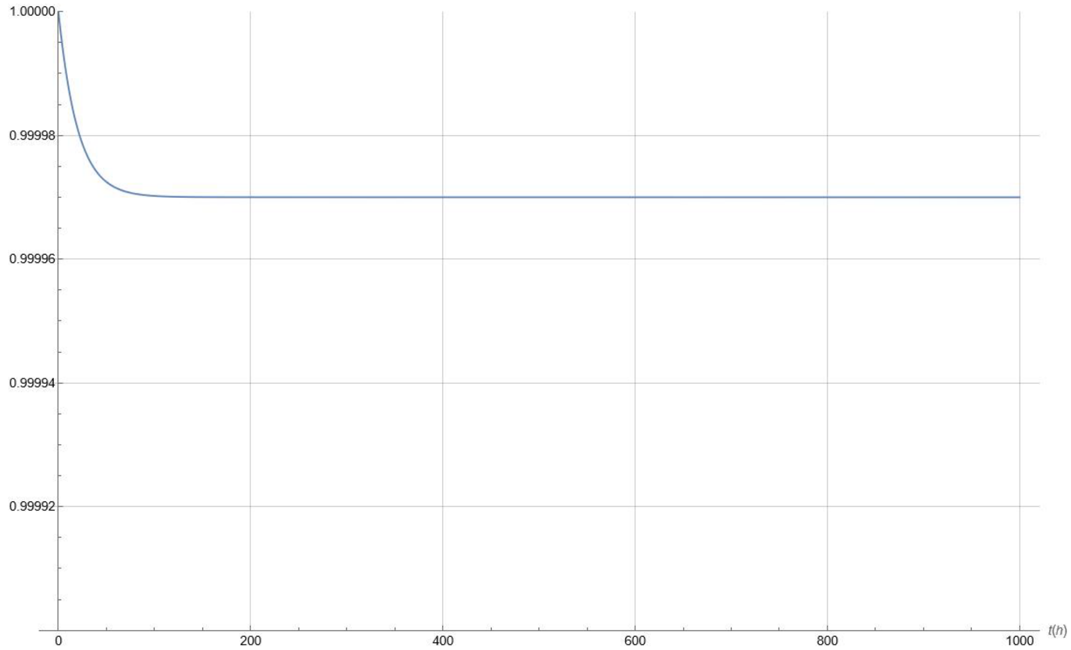

Figure 17. Graphic representation of the $\boldsymbol{R_O(t)}$ for the model illustrated in Fig. 14 (new value interference impact factors).

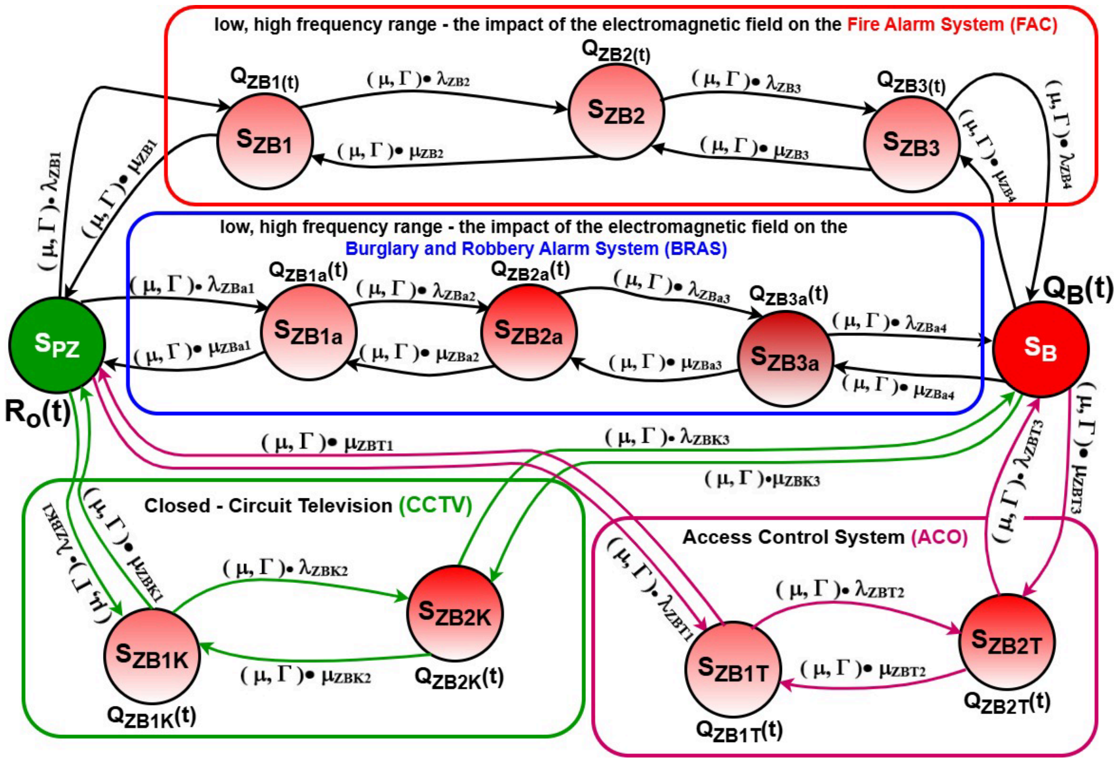

Figure 18. Operation model for an IESS used to protect facilities and vast areas classified as SCI. For reasons associated with protecting facilities classified as SCI, the IESS was supplemented by two security systems, CCTV and ACS, (occupants, accumulated property and documents). For the sake of illustration clarity, failure λ and recovery μ intensities have been colour-marked for two systems: CCTV and ARC.

$$
\begin{gathered}
R_0'(t) = -\mu\Gamma_{\lambda ZB1} \cdot \lambda_{ZB1} \cdot R_0(t) + \mu\Gamma_{\mu ZB1} \cdot \mu_{ZB1} \cdot Q_{ZB1}(t) - \mu\Gamma_{\lambda ZBa1} \cdot \lambda_{ZBa1} \cdot R_0(t) + \mu\Gamma_{\mu ZBa1} \cdot \mu_{ZBa1} \cdot Q_{ZB1a}(t) \\
-\mu\Gamma_{\lambda ZBT1} \cdot \lambda_{ZBT1} \cdot R_0(t) + \mu\Gamma_{\mu ZBT1} \cdot \mu_{ZBT1} \cdot Q_{ZB1T}(t) - \mu\Gamma_{\lambda ZBK1} \cdot \lambda_{ZBK1} \cdot R_0(t) + \mu\Gamma_{\mu ZBK1} \cdot \mu_{ZBK1} \cdot Q_{ZB1K}(t) \\
Q_{ZB1}'(t) = \mu\Gamma_{\lambda ZB1} \cdot \lambda_{ZB1} \cdot R_0(t) - \mu\Gamma_{\mu ZB1} \cdot \mu_{ZB1} \cdot Q_{ZB1}(t) - \mu\Gamma_{\lambda ZB2} \cdot \lambda_{ZB2} \cdot Q_{ZB1}(t) + \mu\Gamma_{\mu ZB2} \cdot \mu_{ZB2} \cdot Q_{ZB2}(t) \\
Q_{ZB2}'(t) = \mu\Gamma_{\lambda ZB2} \cdot \lambda_{ZB2} \cdot Q_{ZB1}(t) - \mu\Gamma_{\mu ZB2} \cdot \mu_{ZB2} \cdot Q_{ZB2}(t) - \mu\Gamma_{\lambda ZB3} \cdot \lambda_{ZB3} \cdot Q_{ZB2}(t) + \mu\Gamma_{\mu ZB3} \cdot \mu_{ZB3} \cdot Q_{ZB3}(t) \\
Q_{ZB3}'(t) = \mu\Gamma_{\lambda ZB3} \cdot \lambda_{ZB3} \cdot Q_{ZB2}(t) - \mu\Gamma_{\mu ZB3} \cdot \mu_{ZB3} \cdot Q_{ZB3}(t) - \mu\Gamma_{\lambda ZB4} \cdot \lambda_{ZB4} \cdot Q_{ZB3}(t) + \mu\Gamma_{\mu ZB4} \cdot \mu_{ZB4} \cdot Q_B(t) \\
Q_{ZB1a}'(t) = \mu\Gamma_{\lambda ZBa1} \cdot \lambda_{ZBa1} \cdot R_0(t) - \mu\Gamma_{\mu ZBa1} \cdot \mu_{ZBa1} \cdot Q_{ZB1a}(t) - \mu\Gamma_{\lambda ZBa2} \cdot \lambda_{ZBa2} \cdot Q_{ZB1a}(t) + \mu\Gamma_{\mu ZBa2} \cdot \mu_{ZBa2} \cdot Q_{ZB2a}(t) \\
Q_{ZB2a}'(t) = \mu\Gamma_{\lambda ZBa2} \cdot \lambda_{ZBa2} \cdot Q_{ZB1a}(t) - \mu\Gamma_{\mu ZBa2} \cdot \mu_{ZBa2} \cdot Q_{ZB2a}(t) - \mu\Gamma_{\lambda ZBa3} \cdot \lambda_{ZBa3} \cdot Q_{ZB2a}(t) + \mu\Gamma_{\mu ZBa3} \cdot \mu_{ZBa3} \cdot Q_{ZB3a}(t) \\
Q_{ZB3a}'(t) = \mu\Gamma_{\lambda ZBa3} \cdot \lambda_{ZBa3} \cdot Q_{ZB2a}(t) - \mu\Gamma_{\mu ZBa3} \cdot \mu_{ZBa3} \cdot Q_{ZB3a}(t) - \mu\Gamma_{\lambda ZBa4} \cdot \lambda_{ZBa4} \cdot Q_{ZB3a}(t) + \mu\Gamma_{\mu ZBa4} \cdot \mu_{ZBa4} \cdot Q_B(t) \\
Q_{ZB1T}'(t) = \mu\Gamma_{\lambda ZBT1} \cdot \lambda_{ZBT1} \cdot R_0(t) - \mu\Gamma_{\mu ZBT1} \cdot \mu_{ZBT1} \cdot Q_{ZB1T}(t) - \mu\Gamma_{\lambda ZBT2} \cdot \lambda_{ZBT2} \cdot Q_{ZB1T}(t) + \mu\Gamma_{\mu ZBT2} \cdot \mu_{ZBT2} \cdot Q_{ZB2T}(t) \\
Q_{ZB2T}'(t) = \mu\Gamma_{\lambda ZBT2} \cdot \lambda_{ZBT2} \cdot Q_{ZB1T}(t) - \mu\Gamma_{\mu ZBT2} \cdot \mu_{ZBT2} \cdot Q_{ZB2T}(t) - \mu\Gamma_{\lambda ZBT3} \cdot \lambda_{ZBT3} \cdot Q_{ZB2T}(t) + \mu\Gamma_{\mu ZBT3} \cdot \mu_{ZBT3} \cdot Q_B(t) \\
Q_{ZB1K}'(t) = \mu\Gamma_{\lambda ZBK1} \cdot \lambda_{ZBK1} \cdot R_0(t) - \mu\Gamma_{\mu ZBK1} \cdot \mu_{ZBK1} \cdot Q_{ZB1K}(t) - \mu\Gamma_{\lambda ZBK2} \cdot \lambda_{ZBK2} \cdot Q_{ZB1K}(t) + \mu\Gamma_{\mu ZBK2} \cdot \mu_{ZBK2} \cdot Q_{ZB2K}(t) \\
Q_{ZB2K}'(t) = \mu\Gamma_{\lambda ZBK2} \cdot \lambda_{ZBK2} \cdot Q_{ZB1K}(t) - \mu\Gamma_{\mu ZBK2} \cdot \mu_{ZBK2} \cdot Q_{ZB2K}(t) - \mu\Gamma_{\lambda ZBK3} \cdot \lambda_{ZBK3} \cdot Q_{ZB2K}(t) + \mu\Gamma_{\mu ZBK3} \cdot \mu_{ZBK3} \cdot Q_B(t) \\
Q_B'(t) = \mu\Gamma_{\lambda ZB4} \cdot \lambda_{ZB4} \cdot Q_{ZB3}(t) - \mu\Gamma_{\mu ZB4} \cdot \mu_{ZB4} \cdot Q_B(t) + \mu\Gamma_{\lambda ZBa4} \cdot \lambda_{ZBa3} \cdot Q_{ZB3a}(t) - \mu\Gamma_{\mu ZBa4} \cdot \mu_{ZBa4} \cdot Q_B(t) + \\
+\mu\Gamma_{\lambda ZBT3} \cdot \lambda_{ZBT3} \cdot Q_{ZB2T}(t) - \mu\Gamma_{\mu ZBT3} \cdot \mu_{ZBT3} \cdot Q_B(t) + \mu\Gamma_{\lambda ZBK3} \cdot \lambda_{ZBK3} \cdot Q_{ZB2K}(t) - \mu\Gamma_{\mu ZBK3} \cdot \mu_{ZBK3} \cdot Q_B(t)
\end{gathered} \tag{7}
$$

Assuming the baseline conditions:

$$
\begin{gathered}
R_0(0) = 1 \\
Q_{ZB1}(0) = Q_{ZB2}(0) = Q_{ZB3}(0) = Q_{ZB1a}(0) = Q_{ZB2a}(0) = Q_{ZB3a}(0) = 0 \\
Q_{ZB1K}(0) = Q_{ZB2K}(0) = Q_{ZB1T}(0) = Q_{ZB2T}(0) = Q_B(0) = 0
\end{gathered} \tag{8}
$$

and applying the Laplace transform, the following system of linear equations is obtained:

$$
\begin{gathered}
s \cdot R_0^*(s) - 1 = -\mu\Gamma_{\lambda ZB1} \cdot \lambda_{ZB1} \cdot R_0^*(s) + \mu\Gamma_{\mu ZB1} \cdot \mu_{ZB1} \cdot Q_{ZB1}^*(s) - \mu\Gamma_{\lambda ZBa1} \cdot \lambda_{ZBa1} \cdot R_0^*(s) + \mu\Gamma_{\mu ZBa1} \cdot \mu_{ZBa1} \cdot Q_{ZB1a}^*(s) \\
-\mu\Gamma_{\lambda ZBT1} \cdot \lambda_{ZBT1} \cdot R_0^*(s) + \mu\Gamma_{\mu ZBT1} \cdot \mu_{ZBT1} \cdot Q_{ZB1T}^*(s) - \mu\Gamma_{\lambda ZBK1} \cdot \lambda_{ZBK1} \cdot R_0^*(s) + \mu\Gamma_{\mu ZBK1} \cdot \mu_{ZBK1} \cdot Q_{ZB1K}^*(s) \\
s \cdot Q_{ZB1}^*(s) = \mu\Gamma_{\lambda ZB1} \cdot \lambda_{ZB1} \cdot R_0^*(s) - \mu\Gamma_{\mu ZB1} \cdot \mu_{ZB1} \cdot Q_{ZB1}^*(s) - \mu\Gamma_{\lambda ZB2} \cdot \lambda_{ZB2} \cdot Q_{ZB1}^*(s) + \mu\Gamma_{\mu ZB2} \cdot \mu_{ZB2} \cdot Q_{ZB2}^*(s) \\
s \cdot Q_{ZB2}^*(s) = \mu\Gamma_{\lambda ZB2} \cdot \lambda_{ZB2} \cdot Q_{ZB1}^*(s) - \mu\Gamma_{\mu ZB2} \cdot \mu_{ZB2} \cdot Q_{ZB2}^*(s) - \mu\Gamma_{\lambda ZB3} \cdot \lambda_{ZB3} \cdot Q_{ZB2}^*(s) + \mu\Gamma_{\mu ZB3} \cdot \mu_{ZB3} \cdot Q_{ZB3}^*(s) \\
s \cdot Q_{ZB3}^*(s) = \mu\Gamma_{\lambda ZB3} \cdot \lambda_{ZB3} \cdot Q_{ZB2}^*(s) - \mu\Gamma_{\mu ZB3} \cdot \mu_{ZB3} \cdot Q_{ZB3}^*(s) - \mu\Gamma_{\lambda ZB4} \cdot \lambda_{ZB4} \cdot Q_{ZB3}^*(s) + \mu\Gamma_{\mu ZB4} \cdot \mu_{ZB4} \cdot Q_B^*(s) \\
s \cdot Q_{ZB1a}^*(s) = \mu\Gamma_{\lambda ZBa1} \cdot \lambda_{ZBa1} \cdot R_0^*(s) - \mu\Gamma_{\mu ZBa1} \cdot \mu_{ZBa1} \cdot Q_{ZB1a}^*(s) - \mu\Gamma_{\lambda ZBa2} \cdot \lambda_{ZBa2} \cdot Q_{ZB1a}^*(s) + \mu\Gamma_{\mu ZBa2} \cdot \mu_{ZBa2} \cdot Q_{ZB2a}^*(s) \\
s \cdot Q_{ZB2a}^*(s) = \mu\Gamma_{\lambda ZBa2} \cdot \lambda_{ZBa2} \cdot Q_{ZB1a}^*(s) - \mu\Gamma_{\mu ZBa2} \cdot \mu_{ZBa2} \cdot Q_{ZB2a}^*(s) - \mu\Gamma_{\lambda ZBa3} \cdot \lambda_{ZBa3} \cdot Q_{ZB2a}^*(s) + \mu\Gamma_{\mu ZBa3} \cdot \mu_{ZBa3} \cdot Q_{ZB3a}^*(s) \\
s \cdot Q_{ZB3a}^*(s) = \mu\Gamma_{\lambda ZBa3} \cdot \lambda_{ZBa3} \cdot Q_{ZB2a}^*(s) - \mu\Gamma_{\mu ZBa3} \cdot \mu_{ZBa3} \cdot Q_{ZB3a}^*(s) - \mu\Gamma_{\lambda ZBa4} \cdot \lambda_{ZBa4} \cdot Q_{ZB3a}^*(s) + \mu\Gamma_{\mu ZBa4} \cdot \mu_{ZBa4} \cdot Q_B^*(s) \\
s \cdot Q_{ZB1T}^*(s) = \mu\Gamma_{\lambda ZBT1} \cdot \lambda_{ZBT1} \cdot R_0^*(s) - \mu\Gamma_{\mu ZBT1} \cdot \mu_{ZBT1} \cdot Q_{ZB1T}^*(s) - \mu\Gamma_{\lambda ZBT2} \cdot \lambda_{ZBT2} \cdot Q_{ZB1T}^*(s) + \mu\Gamma_{\mu ZBT2} \cdot \mu_{ZBT2} \cdot Q_{ZB2T}^*(s) \\
s \cdot Q_{ZB2T}^*(s) = \mu\Gamma_{\lambda ZBT2} \cdot \lambda_{ZBT2} \cdot Q_{ZB1T}^*(s) - \mu\Gamma_{\mu ZBT2} \cdot \mu_{ZBT2} \cdot Q_{ZB2T}^*(s) - \mu\Gamma_{\lambda ZBT3} \cdot \lambda_{ZBT3} \cdot Q_{ZB2T}^*(s) + \mu\Gamma_{\mu ZBT3} \cdot \mu_{ZBT3} \cdot Q_B^*(s) \\
s \cdot Q_{ZB1K}^*(s) = \mu\Gamma_{\lambda ZBK1} \cdot \lambda_{ZBK1} \cdot R_0^*(s) - \mu\Gamma_{\mu ZBK1} \cdot \mu_{ZBK1} \cdot Q_{ZB1K}^*(s) - \mu\Gamma_{\lambda ZBK2} \cdot \lambda_{ZBK2} \cdot Q_{ZB1K}^*(s) + \mu\Gamma_{\mu ZBK2} \cdot \mu_{ZBK2} \cdot Q_{ZB2K}^*(s) \\
s \cdot Q_{ZB2K}^*(s) = \mu\Gamma_{\lambda ZBK2} \cdot \lambda_{ZBK2} \cdot Q_{ZB1K}^*(s) - \mu\Gamma_{\mu ZBK2} \cdot \mu_{ZBK2} \cdot Q_{ZB2K}^*(s) - \mu\Gamma_{\lambda ZBK3} \cdot \lambda_{ZBK3} \cdot Q_{ZB2K}^*(s) + \mu\Gamma_{\mu ZBK3} \cdot \mu_{ZBK3} \cdot Q_B^*(s) \\
s \cdot Q_B^*(s) = \mu\Gamma_{\lambda ZB4} \cdot \lambda_{ZB4} \cdot Q_{ZB3}^*(s) - \mu\Gamma_{\mu ZB4} \cdot \mu_{ZB4} \cdot Q_B^*(s) + \mu\Gamma_{\lambda ZBa4} \cdot \lambda_{ZBa3} \cdot Q_{ZB3a}^*(s) - \mu\Gamma_{\mu ZBa4} \cdot \mu_{ZBa4} \cdot Q_B^*(s) + \\
+\mu\Gamma_{\lambda ZBT3} \cdot \lambda_{ZBT3} \cdot Q_{ZB2T}^*(t) - \mu\Gamma_{\mu ZBT3} \cdot \mu_{ZBT3} \cdot Q_B^*(t) + \mu\Gamma_{\lambda ZBK3} \cdot \lambda_{ZBK3} \cdot Q_{ZB2K}^*(t) - \mu\Gamma_{\mu ZBK3} \cdot \mu_{ZBK3} \cdot Q_B^*(t)
\end{gathered} \tag{9}
$$

Further analysis in relation to the model illustrated in Fig. 17 was conducted assuming the following intensities of transition between distinguished states:

$$\lambda_{ZB1} = 0{,}000001[1/h]\,,\ \lambda_{ZB2} = 0{,}0000008[1/h]\,,\ \lambda_{ZB3} = 0{,}0000006[1/h]\,,\ \lambda_{ZB4} = 0{,}0000004[1/h]\,,$$

$$\mu_{ZB1} = 0{,}1[1/h]\,,\ \mu_{ZB2} = 0{,}1[1/h]\,,\ \mu_{ZB3} = 0{,}1[1/h]\,,\ \mu_{ZB4} = 0{,}1[1/h]\,,$$

$$\lambda_{ZBa1} = 0{,}000001[1/h]\,,\ \lambda_{ZBa2} = 0{,}0000008[1/h]\,,\ \lambda_{ZBa3} = 0{,}0000006[1/h]\,,\ \lambda_{ZBa4} = 0{,}0000004[1/h]\,,$$

$$\mu_{ZBa1} = 0{,}1[1/h]\,,\ \mu_{ZBa2} = 0{,}1[1/h]\,,\ \mu_{ZBa3} = 0{,}1[1/h]\,,\ \mu_{ZBa4} = 0{,}1[1/h]\,,$$

$$\lambda_{ZBT1} = 0{,}000001[1/h]\,,\ \lambda_{ZBT2} = 0{,}0000008[1/h]\,,\ \lambda_{ZBT3} = 0{,}0000006[1/h]\,,$$

$$\mu_{ZBT1} = 0{,}1[1/h]\,,\ \mu_{ZBT2} = 0{,}1[1/h]\,,\ \mu_{ZBT3} = 0{,}1[1/h]\,,$$

$$\lambda_{ZBK1} = 0{,}000001[1/h]\,,\ \lambda_{ZBK2} = 0{,}0000008[1/h]\,,\ \lambda_{ZBK3} = 0{,}0000006[1/h]\,,$$

$$\mu_{ZBK1} = 0{,}1[1/h]\,,\ \mu_{ZBK2} = 0{,}1[1/h]\,,\ \mu_{ZBK3} = 0{,}1[1/h]\,,$$

$$\mu\Gamma_{\lambda ZB1} = \mu\Gamma_{\lambda ZB2} = \mu\Gamma_{\lambda ZB3} = \mu\Gamma_{\lambda ZB4} = 0{,}5[1/h]\,,$$

$$\mu\Gamma_{\mu ZB1} = \mu\Gamma_{\mu ZB2} = \mu\Gamma_{\mu ZB3} = \mu\Gamma_{\mu ZB4} = 0{,}5[1/h]\,,$$

$$\mu\Gamma_{\lambda ZBa1} = \mu\Gamma_{\lambda ZBa2} = \mu\Gamma_{\lambda ZBa3} = \mu\Gamma_{\lambda ZBa4} = 0{,}5[1/h]\,,$$

$$\mu\Gamma_{\mu ZBa1} = \mu\Gamma_{\mu ZBa2} = \mu\Gamma_{\mu ZBa3} = \mu\Gamma_{\mu ZBa4} = 0{,}5[1/h]\,,$$

$$\mu\Gamma_{\lambda ZBk1} = \mu\Gamma_{\lambda ZBk2} = \mu\Gamma_{\lambda ZBk3} = 0{,}5[1/h]\,,$$

$$\mu\Gamma_{\mu ZBk1} = \mu\Gamma_{\mu ZBk2} = \mu\Gamma_{\mu ZBk3} = 0{,}5[1/h]\,,$$

$$\mu\Gamma_{\lambda ZBt1} = \mu\Gamma_{\lambda ZBt2} = \mu\Gamma_{\lambda ZBt3} = 0{,}5[1/h]\,,$$

$$\mu\Gamma_{\mu ZBt1} = \mu\Gamma_{\mu ZBt2} = \mu\Gamma_{\mu ZBt3} = 0{,}5[1/h].$$

The research duration was assumed similarly to the previous model, i.e., as 1 year, i.e., $t = 8760[h]$.

Using the system of equations (9), the following is obtained for the above input values assumed for the simulation:

$$R_0(t) = 0.99996 - 4.7574 \cdot 10^{-14} \cdot e^{-0.2 \cdot t} - 0.045147 \cdot e^{-0.0552129 \cdot t} -$$

$$e^{(-0.0455998\text{-}0.00101709 \cdot i) \cdot t} \cdot \Big((\text{-}0.086413 + 0.027085 \cdot i) - (0.086413 + 0.027085 \cdot i) \cdot e^{(0.00203419 \cdot i) \cdot t}\Big) -$$

$$e^{(-0.054476\text{-}0.0025664 \cdot i) \cdot t} \cdot \Big((0.045765 + 0.0136108 \cdot i) + (0.045765 \text{ - } 0.0136108 \cdot i) \cdot e^{(0.0051328 \cdot i) \cdot t}\Big) -$$

$$e^{(-0.0464583\text{-}0.00287759 \cdot i) \cdot t} \cdot \Big((\text{-}0.0530758 + 0.0690143 \cdot i) - (0.0530758 + 0.0690143 \cdot i) \cdot e^{(0.00575517 \cdot i) \cdot t}\Big) -$$

$$e^{(-0.048061\text{-}0.00424986 \cdot i) \cdot t} \cdot \Big((\text{-}0.00430306 + 0.0784455 \cdot i) - (0.00430306 + 0.0784455 \cdot i) \cdot e^{(0.00849972 \cdot i) \cdot t}\Big) -$$

$$e^{(\text{-}0.0525781\text{-}0.00430529 \cdot i) \cdot t} \cdot \Big((0.0443337 + 0.0329515 \cdot i) + (0.0443337 \text{ - } 0.0329515 \cdot i) \cdot e^{(0.00861057 \cdot i) \cdot t}\Big) -$$

$$e^{(\text{-}0.0502233\text{-}0.00483118 \cdot i) \cdot t} \cdot \Big((0.0310998 + 0.058784 \cdot i) + (0.0310998 \text{ - } 0.058784 \cdot i) \cdot e^{(0.00966235 \cdot i) \cdot t}\Big)$$

The end result (for $\boldsymbol{t = 8760[h]}$) is: $\boldsymbol{R_O = 0{,}99996}$.

Fig. 19 contains a graphic representation of the $\boldsymbol{R_O(t)}$ function.

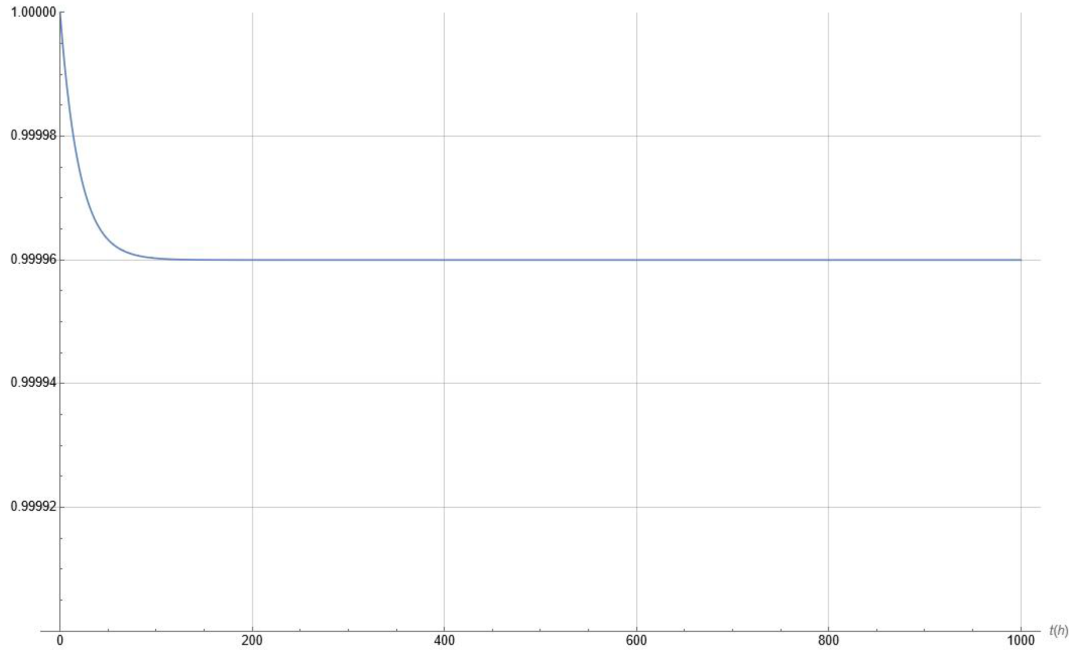

Figure 19. Graphic representation of the $\boldsymbol{R_O(t)}$ for the model illustrated in Fig. 17.

In order to check the correctness of the developed model, the disturbance impact coefficients were changed to the following value:

$$\mu\Gamma_{\lambda ZB1} = \mu\Gamma_{\lambda ZB2} = \mu\Gamma_{\lambda ZB3} = \mu\Gamma_{\lambda ZB4} = 0{,}75[1/h]$$
$$\mu\Gamma_{\lambda ZBa1} = \mu\Gamma_{\lambda ZBa2} = \mu\Gamma_{\lambda ZBa3} = \mu\Gamma_{\lambda ZBa4} = 0{,}75[1/h]$$
$$\mu\Gamma_{\lambda ZBk1} = \mu\Gamma_{\lambda ZBk2} = \mu\Gamma_{\lambda ZBk3} = 0{,}75[1/h]$$
$$\mu\Gamma_{\lambda ZBt1} = \mu\Gamma_{\lambda ZBt2} = \mu\Gamma_{\lambda ZBt3} = 0{,}75[1/h]$$

For the assumed values, calculations were performed again (including Laplace transformations), which enabled the determination of the function dependencies $R_O(t)$ - Fig. 20. The obtained graphical form confirms the correctness of the developed model.

The presented modelling of integrated electronic security systems, taking into account the impact of electromagnetic interference, enables a quantitative evaluation of different technical solutions of such technical objects susceptible to interference. This enables minimising the impact of electromagnetic interference on the operation of all IESSs, particularly detection mains, circuits and lines with hooked-up sensors that detect various distinctive quantities – e,g., smoke, temperature, radiation in fire sensors or motion and motion sensor characteristic zone violation.

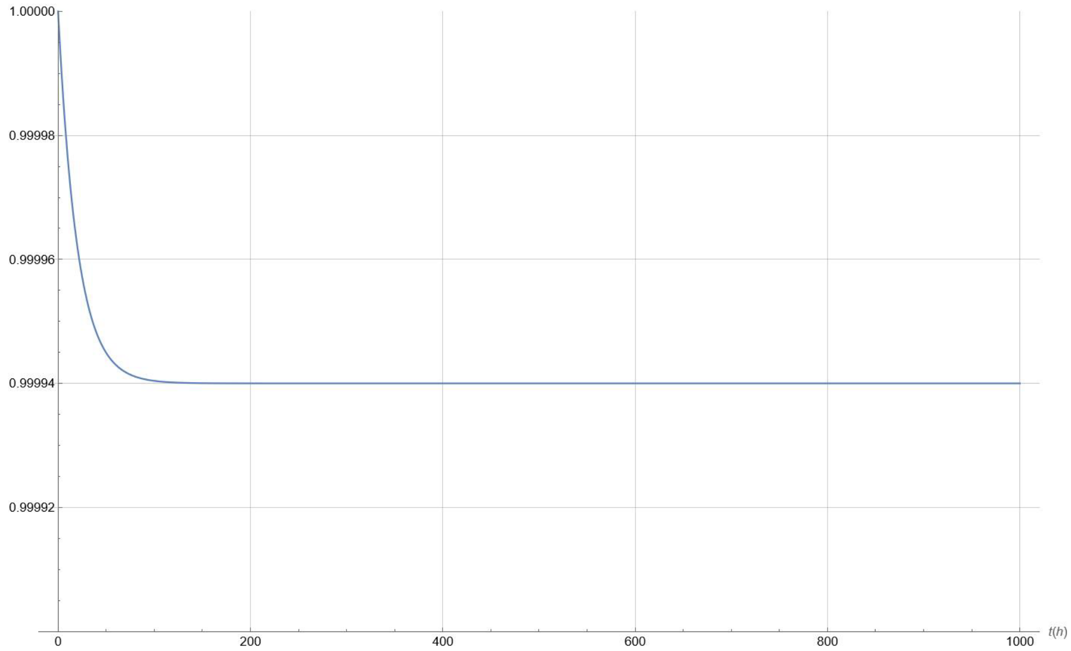

Figure 20. Graphic representation of the $\boldsymbol{R_O(t)}$ for the model illustrated in Fig. 17 (new value interference impact factors).

6. Conclusion

The conducted functional analysis covering integrated electronic security systems in a railway transport environment enabled a conclusion that there are numerous sources of electromagnetic interference acting upon them (the so-called electro-smog that we encounter in everyday life and the surrounding natural environment). Measurements taken allowed the authors to determine numerical values of electromagnetic interference impacting IESS functionality. In turn, an investigation of measurement results warranted determining the frequency range at which the permissible strength values of the electric (E) and magnetic (H) fields (defined by relevant standards applicable for the general environment, including transport) were exceeded. For this reason, it seemed justified to subject IESS to a reliability and operational analysis. This was executed for two different operating modes of such security systems. Operation process modelling, taking into account measurement results for both system types enabled determining relationships that allowed to calculate the probabilities of both technical object types remaining in a state of full fitness. Such a technical condition enables satisfying all pre-engineered operational assumptions, in other words, it it enables the detection of hazards, the implementation of the alarm process, and, in the case of fixed fire extinguishing devices, the initiation of extinguishing actions. This, in turn, enables determining the validity of employing specific technical solutions in internal IESS structures that increase the probability of a system staying in the state of full fitness, even when impacted by electromagnetic interference. Studying the impact of electromagnetic interference on IESS always requires considering frequency ranges of such interference within a given natural environment depending on various propagation methods – e.g., radiation or conduction. An IESS designer should take different methods of counteracting such interference already at the engineering stage by applying the so-called electromagnetic compatibility pyramid. Diagnosing such an electromagnetic environment is also a crucial issue when it comes to operating such security systems within a given area (a specific environment). In the course of the IESS operation process, the natural electromagnetic environment is most often further degraded by the introduction of additional utility signal transmitters (e.g., mobile telephony, Wi-Fi, radio or TV broadcasting stations, radar stations, etc.). The addition of such radiation sources usually requires specific permits covering individual areas, e.g., transport. Particular attention should be paid to unintentional electromagnetic radiation sources (stationary and non-stationary) that may be encountered within a given area – this includes interference from locomotives, electric locomotives, supply traction lines or an industrial power grid. Such a type of electromagnetic interference is particularly dangerous throughout the entire IESS operation process, since a designer might not have the information (E and H field measurements) on such interference sources. The developed method may be employed both in the case of integrated electronic security systems operated within critical infrastructure facilities, as well as within public facilities.

As part of their further research on the impact of electromagnetic interference on IESSs, the authors of this paper intend to expand the study scope with the impact of pulsed interference sources on the operation process, not only of these technical objects. Pulsed electromagnetic interference encountered in a natural environment, e.g., lightning phenomena, current drawn from a contact line when starting-up an electric locomotive or deliberate exposure to high-power pulses, as well as industrial power grid short circuits are characterised by a broad spectrum of electromagnetic interference. Such a pulsed interference process within a given natural environment is a function of rise time and interference duration. Unintentional signals of varying interference frequencies impact an IESS over a relatively short period of time. Therefore, these security systems should be fitted with additional redundant element that respond to electromagnetic interference, often not encountered in the general natural environment.

Acknowledgment

This paper was co-financed under the research grant of the Warsaw University of Technology supporting the scientific activity in the discipline of Civil Engineering, Geodesy and Transport.

References

1. Przesmycki, R, Wnuk M. Susceptibility of it devices to HPM pulse. *International Journal of Safety and Security Engineering* 2018; 8: 223-233. https://doi.org/10.2495/SAFE-V8-N2-223-233.
2. Kierzkowski A, Kisiel T, Uchroński P. Simulation Model of Airport Security Lanes with Power Consumption Estimation. *Energies* 2021; 14: 6725. https://doi.org/10.3390/en14206725.
3. Mach V, Kovář S, Valouch J, Adámek M, Silva RMS. Threshold levels of electromagnetic susceptibility for unarmed air vehicles. In *Proceedings of the 2017 Progress in Electromagnetics Research Symposium—Fall (PIERS—FALL)*, Singapore, 19–22 November 2017; pp. 2483-2488. https://doi.org/10.1109/PIERS-FALL.2017.8293553.
4. Kuryło K, Sabat W, Klepacki D, Kamuda K. Comparison of Two Measurement Methods for the Emission of Radiated Disturbances Generated by LED Drivers. *Energies* 2022; 15: 24. https://doi.org/10.3390/en15249372.
5. Wan, J. Research on Intelligent Detection and Improvement Technology of Urban Rail Transit Electromagnetic Compatibility. *Journal of Physics: Conference Series* 2021; 1982: 012037. https://doi.org/10.1088/1742-6596/1982/1/012037.
6. Firlej A, Musial S, Kubiak I. Data Immunity in Near Field Radio Frequency Communication Systems—NFC as an Aspect of Electromagnetic Information Security. *Applied Sciences* 2024; 14: 13. https://doi.org/10.3390/app14135854.
7. Lewandowski J, Młynarski S, Pilch R, Smolnik M, Szybka J, Wiązania G. An evaluation method of preventive renewal strategies of railway vehicles selected parts. *Eksploatacja i Niezawodnosc – Maintenance and Reliability* 2021; 23(4). https://doi.org/10.17531/ein.2021.4.10.
8. Kovář S, Valouch J, Urbančoková H, Adámek M. Impact of security cameras on electromagnetic environment in far and near-field. In *Proceedings of the 2016 International Conference on Information and Digital Technologies (IDT)*, Rzeszów, Poland, 5–7 July 2016; pp. 156-159. https://doi.org/10.1109/DT.2016.7557166.
9. Paś J, Rosiński A, Wetoszka P, Białek K, Klimczak T, Siergiejczyk M. Assessment of the Impact of Emitted Radiated Interference Generated by a Selected Rail Traction Unit on the Operating Process of Trackside Video Monitoring Systems. *Electronics* 2022; 11: 16. https://doi.org/10.3390/electronics11162554.
10. Aron C, Florin M. Current Approaches in Traffic Lane Detection: A minireview. *The Archives of Automotive Engineering – Archiwum Motoryzacij* 2024; 104: 19-47.
11. Xu Z, Lei C, Yan F. Electromagnetic safety evaluation of Advanced Driving Assistance System in the anechoic chamber. In *Proceedings of the Asia-Pacific International Symposium on Electromagnetic Compatibility (APEMC)*, Beijing, China, 8–11 May 2022; pp. 119-122.
12. Cabello MR, Fernández S, Pous M, Pascual-Gil E, Angulo LD, López P, Riu PJ, Gutierrez GG, Mateos D, Poyatos D, Fernandez M,

Alvarez J, Pantoja M, Añón M, Silva F, Bretones AR, Trallero R, Nuño L, Escot D, Martin RG, Garcia SG. SIVA UAV: A Case Study for the EMC Analysis of Composite Air Vehicles. *IEEE Transactions on Electromagnetic Compatibility* 2017; 59: 1103-1113.

13. Hu X, Zhou S, Chen T, Ghiasi M. Optimal energy management of a DC power traction system in an urban electric railway network with dogleg method. *Energy Sources, Part A: Recovery, Utilization, and Environmental Effects*, 2021, DOI: 10.1080/15567036.2021.1877373.
14. Kochan A, Daszczuk W B, Grabski W, Karolak J. Formal Verification of the European Train Control System (ETCS) for Better Energy Efficiency Using a Timed and Asynchronous Model. *Energies* 2023; 16(8). https://doi.org/10.3390/en16083602.
15. Smolenski R, Lezynski P, Bojarski J, Drozdz W, Long LC. Electromagnetic compatibility assessment in multiconverter power systems—Conducted interference issues. *Measurement* 2020; 165: 108119.
16. 06 Series of Amendments to UN Regulation No. 10 (Electromagnetic compatibility) "Uniform Provisions Concerning the Approval of Vehicles with Regard to Electromagnetic Compatibility", 20 November 2019. Available online: https://unece.org/fileadmin/DAM/trans/main/wp29/wp29regs/2019/E-ECE-324-Add.9-Rev.6.pdf [accessed 8 November 2024].
17. Sakharov KY, Sukhov AV, Ugolev VL, Gurevich YM. Study of UWB Electromagnetic Pulse Impact on Commercial Unmanned Aerial Vehicle. In *Proceedings of the 2018 International Symposium on Electromagnetic Compatibility (EMC EUROPE)*, Amsterdam, The Netherlands, 27–30 August 2018; pp. 40-43.
18. Garcia SG, Silva F, Escot D, Pascual E, Pantoja,, MF, Riu P, Añón,M,Álvarez J, Cabello M, Pous,M, Fernandez S, Trallero R, Poyatos D, Nuño L. UAVEMI project: Numerical and experimental EM immunity assessment of UAV for HIRF and lightning indirect effects. In *Proceedings of the 2016 ESAWorkshop on Aerospace EMC (Aerospace EMC)*, Valencia, Spain, 23–25 May 2016; pp. 1-5.
19. Ruddle AR, Martin AJM. Adapting Automotive EMC to Meet the Needs of the 21st Century. *IEEE Electromagnetic Compatibility Magazine* 2019; 8: 75-85. DOI: 10.1109/MEMC.2019.8878241.
20. Frank R. Avoiding EMC Problems in Automotive Systems. Electronic Design, 2010. Available online: https://www.electronicdesign.com/markets/automotive/article/21796735/avoiding-emc-problems-in-automotive-systems [accessed 8 November 2024].
21. Corbett F. EMC Challenges in Connected Cars, TTI Europe. The Specialist in Electronic Component Distribution. Available online: https://business-iq.net/assets/3588-emc-challenges-in-connected-cars?open_form=1 [accessed 8 November 2024].
22. Davis S. EMC Poses Challenge for Automotive Electronics. Electronic Design, 2010. Available online: https://www.electronicdesign.com/technologies/power/power-supply/power-electronics-systems/article/21192169/emc-poses-challenge-for-automotiveelectronics [accessed 8 November 2024].
23. Rychlicki M, Kasprzyk Z. Increasing performance of SMS based information systems. *Proceedings of the Ninth International Conference on Dependability and Complex Systems DepCoS-RELCOMEX* 2014; 286: 373-382. https://doi.org/10.1007/978-3-319-07013-1_36.
24. Suproniuk M, Skibko Z, Stachno A. Diagnostics of some parameters of electricity generated in wind farms. *Przegląd Elektrotechniczny* 2019; 95: 105-108.
25. Nie J, Chen X, Shao W, Fang W. Susceptibility of a microcontroller against electrical fast transients disturbances. *Journal of Physics: Conference Series* 2018; 1074: 012117. https://doi.org/10.1088/1742-6596/1074/1/012117.
26. Deutschmann B, Winkler G, Kastner P. Impact of electromagnetic interference on the functional safety of smart power devices for automotive applications. *Elektrotechnik Und Informationstechnik* 2018; 135: 352-359.
27. Hubing TH. Autonomous Vehicles Will Transform the Field of Automotive EMC. In *Proceedings of the IEEE Symposium on Electromagnetic Compatibility, Signal Integrity and Power Integrity (EMC, SI & PI)*, Long Beach, CA, USA, 30 July–3 August 2018; pp. 1-29.
28. Zaklika W.,Sterniczuk D. The importance and directions of electromagnetic compatibility test methodologies development in the aspect of vehicle safety. In *IOP Conference Series: Materials Science and Engineering, Automotive Safety*; IOP Publishing: Bristol, UK, 2022.
29. IEEE Std 1848-2020; IEEE Standard for Techniques and Measurement to Manage Functional Safety and Other Risks with Regards to Electromagnetic Disturbances. Developed by the Standards Development and Education Committee, 2021. Available online: https://ieeexplore.ieee.org/document/9416938 [accessed 8 November 2024].
30. Wu Y.,Huang W. Studies and analysis on unintentional electromagnetic radiation of UAV. In *Proceedings of the 2015 IEEE 6th International Symposium on Microwave, Antenna, Propagation, and EMC Technologies (MAPE)*, Shanghai, China, 28–30 October 2015;

pp. 479-482.

31. May IV, Balashov SY, Vekovshinina SA, Kudrya MA. On assessing electromagnetic field (300 kHz–300 MHz) in a large industrial city on the basis of 3d modeling and instrumental measuring. *Health Risk Analysis* 2017; 3: 21-30. DOI: 10.21668/health.risk/2017.3.03.eng.
32. Perka B. The dissipation of electricity in electric cables under the influence of fire temperatures. *Przegląd Elektrotechniczny* 2021; 97(6): 105-108, https://doi.org/10.15199/48.2021.06.19.
33. Gil I, Fernández-García R. Electromagnetic interference reduction in printed circuit boards by using metamaterials: A conduction and radiation impact analysis. *Journal of Electromagnetic Waves and Applications* 2014; 28: 378-388. https://doi.org/10.1080/09205071.2013.872055.
34. Trip B.; Butnariu V, Vizitiu M, Boitan A, Halunga S. Analysis of compromising video disturbances through power line. *Sensors* 2022; 22: 1. https://doi.org/10.3390/s22010267.
35. Kurnaz C, Mutlu M. Comprehensive radiofrequency electromagnetic field measurements and assessments: A city center example. *Environmental Monitoring and Assessment* 2020; 192: 334. https://doi.org/10.1007/s10661-020-08312-3.
36. Fernández-García R, Gil I. Measurement of the environmental broadband electromagnetic waves in a mid-size European city. *Environmental Research* 2017; 158: 768-772. https://doi.org/10.1016/j.envres.2017.07.040.
37. Armstrong K. Specifying lifecycle electromagnetic and physical environments-to help design and test for EMC for functional safety. In *Proceedings of the 2005 International Symposium on Electromagnetic Compatibility*, Chicago, IL, USA, 8–12 August 2005; Volume 2, pp. 495-500. DOI: 10.1109/ISEMC.2005.1513565.
38. CISPR 25:2021; Vehicles, Boats and Internal Combustion Engines—Radio Disturbance Characteristics—Limits and Methods of Measurement for the Protection of On-Board Receivers. IEC: Geneva, Switzerland, 2021.
39. Diez L, Agüero R, Muñoz L. Electromagnetic Field Assessment as a Smart City Service: The SmartSantander Use-Case. *Sensors* 2017; 17: 1250. https://doi.org/10.3390/s17061250.
40. Ali KJ. Measurements of Electromagnetic Fields Emitted from Cellular Base Stations in Shirqat City. *Tikrit Journal of Engineering Sciences* 2013; 20: 51-61. DOI: https://doi.org/10.25130/tjes.20.1.06.
41. Tosaka T, Taira K, Yamanaka Y, Fukunaga K, Nishikata A, Hattori M. Reconstruction of Printed Image Using Electromagnetic Disturbance from Laser Printer. *IEICE TRANSACTIONS on Communications* 2007; E90-B: 711-715. https://doi.org/10.1093/ietcom/e90-b.3.711.
42. Ott HW. Electromagnetic compatibility engineering. Wiley. 2009. http://dx.doi.org/10.1002/9780470508510.
43. Stawowy M, Perlicki K, Sumiła M. Comparison of uncertainty multilevel models to ensure ITS services. In *Safety and Reliability: Theory and Applications, Proceedings of the European Safety and Reliability Conference ESREL 2017*, Portoroz, Slovenia, 18–22 June 2017; Cepin, M., Bris, R., Eds.; CRC Press/Balkema: London, UK, 2017; pp. 2647-2652.
44. Smolenski R, Lezynski P, Bojarski J, Drozdz W, Choon Long L. Electromagnetic compatibility assessment in multiconverter power systems – Conducted interference issues. *Measurement* 2020; 165: 108119. https://doi.org/10.1016/j.measurement.2020.108119.
45. Chrzan M, Kornaszewski M, Ciszewski T. Renovation of marine telematics objects in the process of exploitation. In *Management Perspective for Transport Telematics*; Springer: Cham, Switzerland, 2018; pp. 337-351.
46. Białoń A, Białek K, Wetoszka P. Analysis of emission tests of electromagnetic disturbancesin diesel-electric locomotives. *2nd International Scientific and Practical Conference "Energy-Optimal Technologies, Logistic and Safety on Transport" (EOT-2019)*. MATEC Web Conf. 2019, 294, 02001.
47. Pinto A, Herrera L-C, Donoso Y, Gutierrez JA. Survey on Intrusion Detection Systems Based on Machine Learning Techniques for the Protection of Critical Infrastructure. *Sensors* 2023; 23: 2415. https://doi.org/10.3390/s23052415.
48. Panagiotis F, Taxiarxchis K, Georgios K, Maglaras L, Ferrag MA. Intrusion Detection in Critical Infrastructures: A Literature Review. *Smart Cities* 2021; 4: 1146-1157. https://doi.org/10.3390/smartcities4030061.
49. Wang W, Mingli W, Sun J. Analysis of Low-Frequency Oscillation in Electric Railways Based on Small-Signal Modeling of Vehicle-Grid System in dq Frame. *IEEE Transactions on Power Electronics* 2015; 30: 5318-5330. https://doi.org/10.1109/TPEL.2015.2388796.
50. Białek K, Wetoszka P. Analysis of Elimination of Electromagnetic Disturbances at Power Ports of Railway Equipment. In *Research Methods and Solutions to Current Transport Problems. ISCT21 2019 Advances in Intelligent Systems and Computing*; Siergiejczyk, M., Krzykowska, K., Eds.; Springer: Cham, Germany, 2020; Volume 1032. https://doi.org/10.1007/978-3-030-27687-4_4.

51. Paś J, Klimczak T, Rosiński A, Stawowy M. The Analysis of the Operational Process of a Complex Fire Alarm System Used in Transport Facilities. *Building Simulation* 2022; 15(4). https://doi.org/10.1007/s12273-021-0790-y.
52. Duer S, Zajkowski K, Harničárová M, Charun H, Bernatowicz D. Examination of Multivalent Diagnoses Developed by a Diagnostic Program with an Artificial Neural Network for Devices in the Electric Hybrid Power Supply System "House on Water". *Energies* 2021; 14: 2153.
53. Yan H, Ma L, Zhao T, Zhang J. Research on repair method of abnormal energy consumption data of lighting and plug based on similar features. *Energy and Buildings* 2022; 268. https://doi.org/10.1016/j.enbuild.2022.112155.
54. Klimczak T, Paś J, Duer S, Rosiński A, Wetoszka P, Białek K, Mazur M. Selected Issues Associated with the Operational and Power Supply Reliability of Fire Alarm Systems. *Energies* 2022; 15(22): 8409. https://doi.org/10.3390/en15228409.
55. Nucci CA, Borghetti A, Napolitano F, Tossani F. Basics of Power Systems Analysis. In: Papailiou K.O. (eds) *Springer Handbook of Power Systems*. Springer, Singapore, 2021. https://doi.org/10.1007/978-981-32-9938-2_5.
56. Sueta HE, Santos SR, Altafim RAC. Protection of Low-Voltage Equipment and Systems. In: Gomes C. (eds) Lightning. *Lecture Notes in Electrical Engineering*, vol 780. Springer, Singapore, 2021. https://doi.org/10.1007/978-981-16-3440-6_5.
57. Alias WNHA, Sujod MZ, Kamari NAM. DC-Link Protection for Grid-Connected Photovoltaic System: A Review. In: Kasruddin Nasir A.N. et al. (eds) In: *ECCE2019. Lecture Notes in Electrical Engineering*, vol 632. Springer, Singapore, 2020. https://doi.org/10.1007/978-981-15-2317-5_61.
58. Jin T, Yu Y, Elsayed E. Reliability and quality control for distributed wind/solar energy integration: a multi-criteria approach, *IIE Transactions* 2015; 47(10): 1122-1138. DOI: 10.1080/0740817X.2015.1009199.
59. Hashemi S, Østergaard J. Methods and strategies for overvoltage prevention in low voltage distribution systems with PV. *IET Renewable Power Generation* 2017; 11: 205-214. https://doi.org/10.1049/iet-rpg.2016.0277.
60. Pawar P, TarunKumar M, Vittal PK. An IoT based Intelligent Smart Energy Management System with accurate forecasting and load strategy for renewable generation. *Measurement* 2020; 152: 107187. https://doi.org/10.1016/j.measurement.2019.107187.
61. Duer S. Assessment of the operation process of wind power plant's equipment with the use of an artificial neural network. *Energies* 2020; 13: 2437, doi:10.3390/en13102437.
62. Rock M. Protection of Selected Cases: PV Systems, Wind Turbines and Railway Systems. In: Gomes C. (eds) *Lightning. Lecture Notes in Electrical Engineering*, vol 780. Springer, Singapore, 2021. https://doi.org/10.1007/978-981-16-3440-6_7.
63. Azghandi MA, Barakati SM. A Temporary Overvoltages Mitigation Strategy for Grid-Connected Photovoltaic Systems Based on Current-Source Inverters. *Iranian Journal of Science and Technology, Transactions of Electrical* Engineering 2020; 44: 1253-1262. https://doi.org/10.1007/s40998-019-00291-7.
64. Chetty L, Singh Y. Reliability Assessment of High Voltage Direct Current Grid Protection Schemes. *Quality and Reliability Engineering International* 2014; 30: 1461-1472. https://doi.org/10.1002/qre.1568.
65. El-kordy M, El-fergany A, Gawad AFA. Various Metaheuristic-Based Algorithms for Optimal Relay Coordination: Review and Prospective. *Archives of Computational Methods in Engineering* 2021; 28: 3621-3629. https://doi.org/10.1007/s11831-020-09516-z.
66. Piersanti S, Orlandi A, Paulis de F. Electromagnetic absorbing materials design by optimization using a machine learning approach. *IEEE Transactions on Electromagnetic Compatibility* 2018: 1-8. DOI: 10.1109/TEMC.2018.2871879.
67. Rolim FBB, Trindade FCL, Rider MJ. Adaptive Protection Methodology for Modern Electric Power Distribution Systems. *Journal of Control, Automation and Electrical Systems* 2021; 32: 1377-1388. https://doi.org/10.1007/s40313-021-00774-1.
68. Cao M-Q, Liu T-T, Zhu Y-H, Shu J-C. Cao M-S. Developing electromagnetic functional materials for green building. *Journal of Building Engineering* 2022; 45. https://doi.org/10.1016/j.jobe.2021.103496.
69. Kossakowski D, Krzykowska K. Application of V2X Technology in Communication between Vehicles and Infrastructure in Chosen Area. In *Research Methods and Solutions to Current Transport Problems, Proceedings of the International Scientific Conference Transport of the 21st Century, Advances in Intelligent Systems and Computing*, Ryn, Poland, 9–12 June 2019; Siergiejczyk, M., Krzykowska, K., Eds.; Springer: Cham, Switzerland, 2020; Volume 1032, pp. 247-256.
70. Park G, Kim S, Park G-K, Lee N. Influence of carbon fiber on the electromagnetic shielding effectiveness of high-performance fiber-reinforced cementitious composites. *Journal of Building Engineering* 2021; 35. https://doi.org/10.1016/j.jobe.2020.101982.

71. Skuza A, Ziemianek S, Suproniuk M. Power System Division—Certain Issues Associated with Shaping Commutation Strategies in Power Substations. *Energies* 2022; 15(9): 7293. https://doi.org/10.3390/en15197293.
72. Borucka A. Maintaining technical readiness in the context of military exploitation systems. *Bulletin of the Polish Academy of Sciences, Technical Sciences* 2023; 71(5). https://doi.org/10.24425/bpasts.2023.146619.
73. Gauder D, Bott A, Gölz J, Lanza G. Simulation uncertainty determination of single flank rolling tests using monte carlo simulation and skin model shapes for zero defect manufacturing of micro gears. *Computers in industry* 2023; 146: 103854. https://doi.org/10.1016/j.compind.2023.103854.
74. Liu Z.,Xu Y, Li Z, Zhai M, Yang W, Lin J, Sun Y. Towards evidence-based fire prevention policy: Uncovering drivers of urban residential fire spread via explainable machine learning. *Developments in the built environment* 2025; 24: 100761. https://doi.org/10.1016/j.dibe.2025.100761.
75. Elhanashi A, Essahraui S, Dini P, Saponara S. Early Fire and Smoke Detection Using Deep Learning: A Comprehensive Review of Models, Datasets, and Challenges. Applied *Sciences* 2025; 15: 10255. https://doi.org/10.3390/app151810255.
76. Yonggang Li, Yaotong Su, Lei Xia, Yuanjin Zhang, Weinong Wu, Longjiang Li. Reliability evaluation of wind power systems by integrating granularity-related latin hypercube sampling with LSTM-based prediction. *Computers in industry* 2025; 173: 104365. ISSN 0166-3615. https://doi.org/10.1016/j.compind.2025.104365.
77. Kasprzyk Z, Rychlicki M. Analysis of Physical Layer Model of WLAN 802.11g Data Transmission Protocol in Wireless Networks Used by Telematic Systems. In *Proceedings of the Ninth International Conference on Dependability and Complex Systems DepCoS-RELCOMEX* , Zamojski Wojciech *[i in.]* (*red.*), Advances in Intelligent Systems and Computing, 2014, vol. 286, Heidelberg, Springer International Publishing, 265-274. DOI:10.1007/978-3-319-07013-1_25.
78. Billinton R, Allan RN. *Reliability evaluation of power systems*. New York: Plenum Press, 1996. https://doi.org/10.1007/978-1-4899-1860-4.
79. Duer S, Woźniak M, Paś J, Zajkowski K, Bernatowicz D, Ostrowski A, Budniak, Z. Reliability Testing of Wind Farm Devices Based on the Mean Time between Failures (MTBF). *Energies* 2023; 16: 1659. https://doi.org/10.3390/en16041659.
80. Kong DP, Lu SX, Ping P. A Risk-Based Method of Deriving Design Fires for Evacuation Safety in Buildings. *Fire Technology* 2017; 53: 771-791. https://doi.org/10.1007/s10694-016-0600-8.
81. Kozłowski E, Borucka A, Oleszczuk P, Jałowiec T. Evaluation of the maintenance system readiness using the semi Markov model taking into account hidden factors. *Eksploatacja i Niezawodność – Maintenance and Reliability* 2023; 25(4). https://doi.org/10.17531/ein/172857.
82. Duer S, Zajkowski K, Harničárová M, Charun H, Bernatowicz D. Examination of Multivalent Diagnoses Developed by a 649 Diagnostic Program with an Artificial Neural Network for Devices in the Electric Hybrid Power Supply System "House on 650 Water". *Energies* 2021; 14: 2153. https://doi.org/10.3390/en14082153.
83. van Coile R.,Hopkin D, Lange D,, Jomaas, G, Bisby L. The Need for Hierarchies of Acceptance Criteria for Probabilistic Risk Assessments in Fire Engineering. *Fire Technology* 2019; 55: 1111-1146.
84. Stawowy M, Perlicki K, Sumiła M. Comparison of uncertainty multilevel models to ensure ITS services. In *Safety and Reliability: Theory and Applications, Proceedings of the European Safety and Reliability Conference ESREL 2017*, Portoroz, Slovenia, 18–22 June 2017; Cepin, M., Bris, R., Eds.; CRC Press/Balkema: London, UK, 2017; pp. 2647-2652.
85. Świderski A, Józwiak A, Jachimowski R. Operational quality measures of vehicles applied for the transport services evaluation using artificial neural networks. *Eksploatacja i Niezawodność – Maintenance and Reliability* 2018; 20: 292-299.
86. Krzykowska-Piotrowska K, Siergiejczyk M. On the Navigation, Positioning and Wireless Communication of the Companion 1127 Robot in Outdoor Conditions. *Energies* 2022; 15: 4936. https://doi.org/10.3390/en15144936.
87. Slowak P, Kaniewski P. Stratified Particle Filter Monocular SLAM. *Remote Sensing* 2021; 13: 3233. https://doi.org/10.3390/rs13163233.
88. Białek R, Wiśnios M, Kuchta M. Badania prototypowego detektora pola magnetycznego, w szczególności impulsów HPEM. *Przegląd Elektrotechniczny* 2019; 95(12): 93-96, 2019, DOI: 10.15199/48.2019.12.18.
89. Duer S, Rokosz K, Zajkowski K, Bernatowicz D, Ostrowski A, Woźniak M, Iqbal A. Intelligent Systems Supporting the Use of Energy Devices and Other Complex Technical Objects: Modeling, Testing, and Analysis of Their Reliability in the Operating Process. *Energies* 2022; 15: 6414.

90. Świderski A, Jóźwiak A, Jachimowski R. Operational quality measures of vehicles applied for the transport services evaluation using artificial neural networks. *Eksploatacja i Niezawodność – Maintenance and Reliability* 2018; 20: 292-299.
91. Andrzejczak K, Bukowski L. A method for estimating the probability distribution of the lifetime for new technical equipment based on expert judgement. *Eksploatacja i Niezawodność – Maintenance and Reliability* 2021; 23: 757-769.
92. Celiński I, Burdzik R, Młyńczak J, Kłaczyński, M. Research on the Applicability of Vibration Signals for Real-Time Train and Track Condition Monitoring. *Sensors* 2022; 22: 2368.
93. Zajkowski K. Two-stage reactive compensation in a three-phase four-wire systems at nonsinusoidal periodic waveforms. *Electric Power Systems Research* 2020; 184: 106296.
94. Zajkowski K, Rusica I, Palkova Z. The use of CPC theory for energy description of two nonlinear receivers. *MATEC Web Conf.* 2018, 178, 09008.
95. Dziula P, Paś J. Low Frequency Electromagnetic Interferences Impact on Transport Security Systems Used in Wide Transport Areas. *International Journal on Marine Navigation and Safety of Sea Transportation* 2018; 12: 251-258. https://doi.org/10.12716/1001.12.02.04.
96. Duer S, Duer R. Diagnostic system with an artificial neural network that determines a diagnostic information for the servicing of a reparable technical object. *Neural Computing and Applications* 2010; 19(5): 755-766. https://doi.org 10.1007/s00521-009-0333-4.
97. Kaniewski P. Extended Kalman Filter with Reduced Computational Demands for Systems with Non-Linear Measurement Models. *Sensors* 2020; 20: 1584. https://doi.org/10.3390/s20061584.
98. Sterniczuk D, Zaklika W, Kozlowski M. Identification Tests of Modern Vehicles' Electromagnetic Environment as Part of the Assessment of Their Functional Safety. *Sensors* 2025; 25: 7. https://doi.org/10.3390/s25010007.
99. Suproniuk M, Skibko Z, Stachno A. Diagnostics of some parameters of electricity generated in wind farms. *Przegląd Elektrotechniczny* 2019; 95: 105-108.

List of important abbreviations and symbols

No.	Full name for abbrevation	Abbr.
1	Alarm Receiving Centre	ARC
2	Electronic Security Systems	ESS
3	European Train Control System	ETCS
4	Global System for Mobile Communications	GSM
5	GSM for Railways	GSM-R
6	State Critical Infrastructure	SCI
7	Intensities of damage	λ
8	Intensities of repairs	μ
9	Railway Institute Test Track Operation Centre	OETD
10	State Fire Service	PSP
11	State of Partial Fitness	S_{ZB}
12	State of Full Fitness	S_{PZ}
13	State of Unfitness	S_B
14	Video Monitoring System	VMS
15	Fire Alarm System	FAS
16	Integrated electronic security systems	IESS
17	Access Control Systems	ACS
18	Closed-Circuit Television	CCTV
19	Intrusion Detection Systems	IDS
20	Audio Warning Systems	AWS
21	State Critical Infrastructure	SCI
22	Alarm Control Panels	ACP
23	Alarm Control Unit	ACU
24	low frequency interference appears in buildings and over a vast area	$\mu \geq 0, \Gamma = 0$
25	only high frequency interference occurs in buildings and over a vast area; low frequency interference is attenuated by anti-destructive filters and elements located in the ACU	$\mu = 0, \Gamma \geq 0$
26	interference in both ranges, low and high frequency, appears in buildings and across large areas	$\mu \geq 0, \Gamma \geq 0$